COMBUSTION OF OIL ON WATER

D. Evans, H. Baum, B. McCaffrey, G. Mulholland, M. Harkleroad and W. Manders
Center for Fire Research, National Bureau of Standards
Gaithersburg, Maryland 20899

ABSTRACT

This report contains the results of measurements performed on both 0.4 m and 0.6 m diameter pool fires produced by burning a layer of Prudhoe Bay crude oil supported by a thermally deep layer of water. Both steady and vigorous burning caused by boiling of the water sublayer were observed. The measured energy release rate for steady burning was about 640 kW/m^2. The emission rate, the size distribution, and specific extinction coefficient were measured for the smoke aerosol produced by the fires. Data were also obtained on the structure of the smoke aerosol by electron microscopy and on emission of CO and CO_2. Analysis of the crude oil burn residue indicated selected depletion of the short chain alkanes and cycloalkanes when compared to the fresh oil. Mono-ring aromatics including benzene, toluene, and xylenes present in the fresh crude were absent in the burn residue. Calculations of the induced air flow into a simulated distribution of 20 fires over a 100 m x 100 m area showed that the maximum inflow velocity near the largest size fire (2.5 m diameter, 3.2 MW) was 1.1 m/s.

BACKGROUND

In 1985, the Center for Fire Research (CFR) at the U.S. National Bureau of Standards (NBS) began studies of oil spill combustion under support from the U.S. Minerals Management Service (MMS). This work seeks to understand the process of oil spill combustion on open waters and in water filled channels formed in broken ice. This work is intended to be a cooperative effort leading to results that may be used to generalize specific measurement of oil spill burn efficiency performed by Smith and Diaz at the EPA-OHMSETT facility in Leonardo, NJ [1]. The scope of the original work has been broaden by added support from Environment Canada and the U.S. Coast Guard to include calculations and measurements related to induced air flow velocities in the area of the fire, burn residue chemical composition, and smoke production from the oil spill burn.

The long range goal of the research program is to provide a means to make quantitative predictions of the fraction of oil in a spill that can be consumed by an in-situ combustion process, the characteristics of the residual oil, and the characteristics of the combustion product flow from the burn. It is hoped that this information may be cast into a form that is readily useable by local officials and oil spill response professionals as part of their decision making process in the event of an oil spill.

As a first step in this research program a framework for detailed study and calculation of the open water oil spill combustion process was formulated by Wichman [2]. It was clear from this initial work that to obtain an overall understanding of oil spill combustion and to produce sound technical quantification of the important effects of combustion, such as the beneficial consumption of oil and detrimental smoke production, closely coordinated experimental and theoretical studies must be conducted. To address many

aspects of the oil spill combustion process, both for confined and unconfined spills, an interdisciplinary research team was assembled within the Center for Fire Research at the U.S. National Bureau of Standards. This team brings together expertise in combustion, fire dynamics, computational fluid flow, particulate measurement, and chemical analysis. All members of the team are contributors to this paper which contains quantitative results for confined oil spill energy release rate, thermal radiation, smoke production, induced air flow, and chemical composition changes between the fresh oil and burn residue.

EXPERIMENTAL FACILITY

Test work in this study was conducted in the CFR large scale testing facility in which a calorimeter hood was used. The experimental facility accommodates oil pool fires up to 0.6 m in diameter. This facility is used cooperatively with studies funded by U.S. Defense Nuclear Agency. A schematic drawing of the instrumented hood is shown in Figure 1. Liquid pool fires are situated under the 2.4 m x 2.4 m collection hood with an adjustable exhaust rate up to about 2 m^3/s (4000 ft^3/min). A tripper plate at the stack inlet insures uniform mixing of combustion products and dilution air before the gases are sampled five duct diameters downstream of the inlet. The mass loss of the burning fuel floated on a deep water layer is monitored using a water cooled load cell with a sensitivity of about 3 grams. Thermal radiation from the fire is measured with a Gardon-type radiometer located several pool diameters from the pan.

Energy release rate from the fire is determined using oxygen consumption calorimetry. This method is based on the fact that the heat of the combustion is about 13 kJ/g of oxygen consumed for all hydrocarbon fuels [3,4]. Thus measurements of O_2 concentration and total flow rate through the stack made downstream of the horseshoe section in the duct are used to calculate the O_2 consumption rate and proportional energy release rate of the fire.

Other measurements in the exhaust duct relate directly to measurement of smoke production and soot particulates. A cascade impactor with seven stages and a backup filter was used for monitoring the aerodynamic size distribution of the aerosol. Quartz fiber filters were used as the collection substrate to minimize the smoke particle bounce that might occur on a flat metal substrate. Particle bounce could be significant for the solid, agglomerate type particles making up the smoke aerosol. Each collection substrate including metal disk and filter were weighed to the nearest 0.01 mg. The sampling flow was about 22 l/min and a conical probe with 0.64 cm orifice was used to insure isokinetic sampling at a velocity of about 10 m/s. The impactor was preheated in a convection oven for thirty minutes and then was rapidly positioned in the stack just before igniting the crude oil pool. This was done to minimize moisture condensation on the impactor stages.

The filter collection system, illustrated in Figure 2, allowed for the sequential collection of three filter samples over the course of a pool fire test. The transfer line, manifold, and filter holders were all heated to match the stack temperature during the burn. This was done to minimize the evaporation/condensation of the smoke aerosol during transport or on the filter and to minimize the thermophoretic driven deposition of particles on the walls. The sample flow, about 10 l/min, and nozzle inlet, 0.48 (3/16 inch), were selected to insure isokinetic sampling. The all glass construction of the filter collection system allowed ready inspection of deposition

He-Ne
LASER

TO PUMP

IMPACTOR

FILTER HOLDER

TO FLOW
CONTROLLER

TC

PITOT TUBE

5D

D

GAS SAMPLING
FOR O_2, CO_2, CO

TC

PLENUM

TRIPPER PLATE

COLLECTION HOOD

TO EXHAUST
STACK

POOL

LOAD CELL
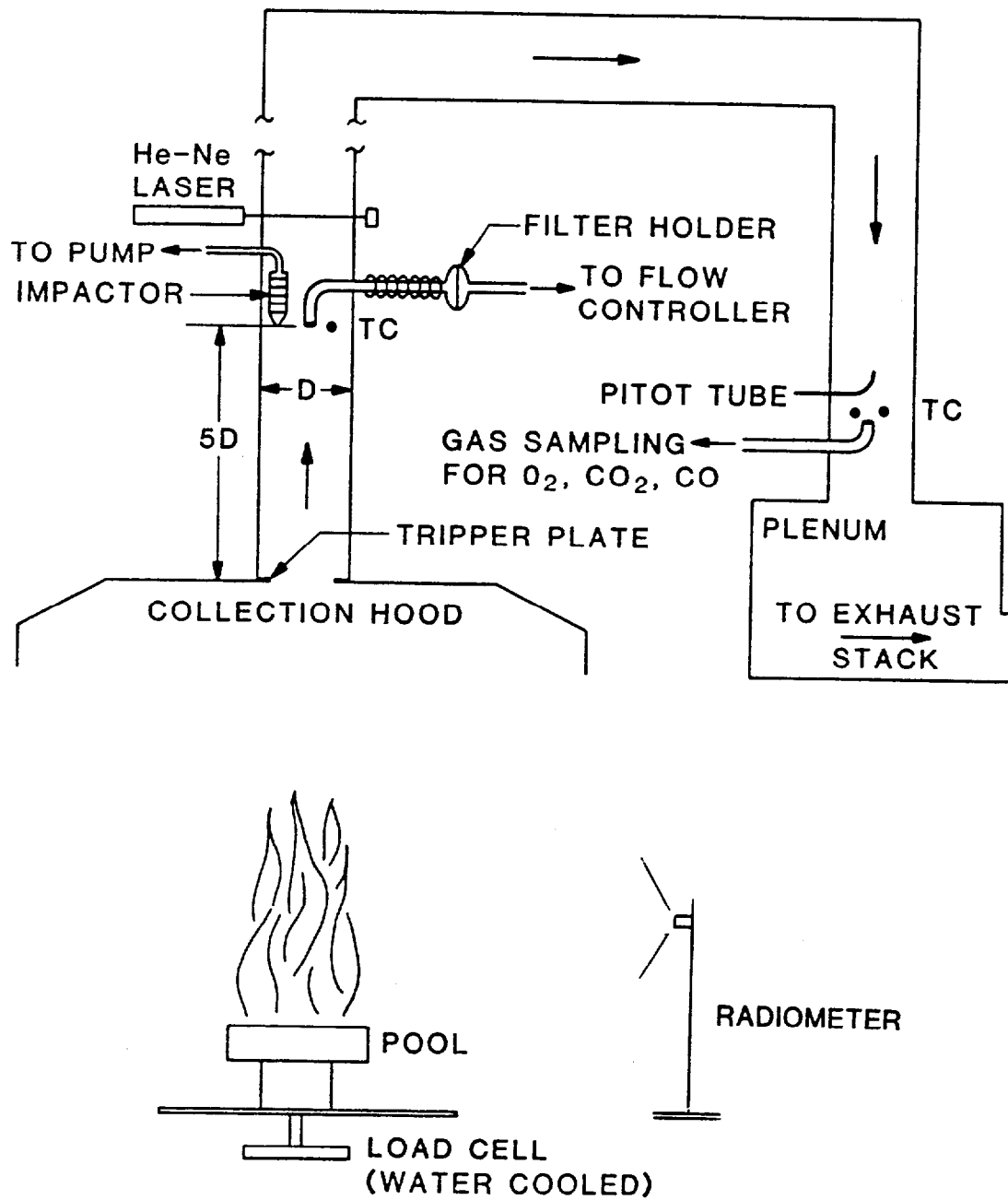(WATER COOLED)

RADIOMETER

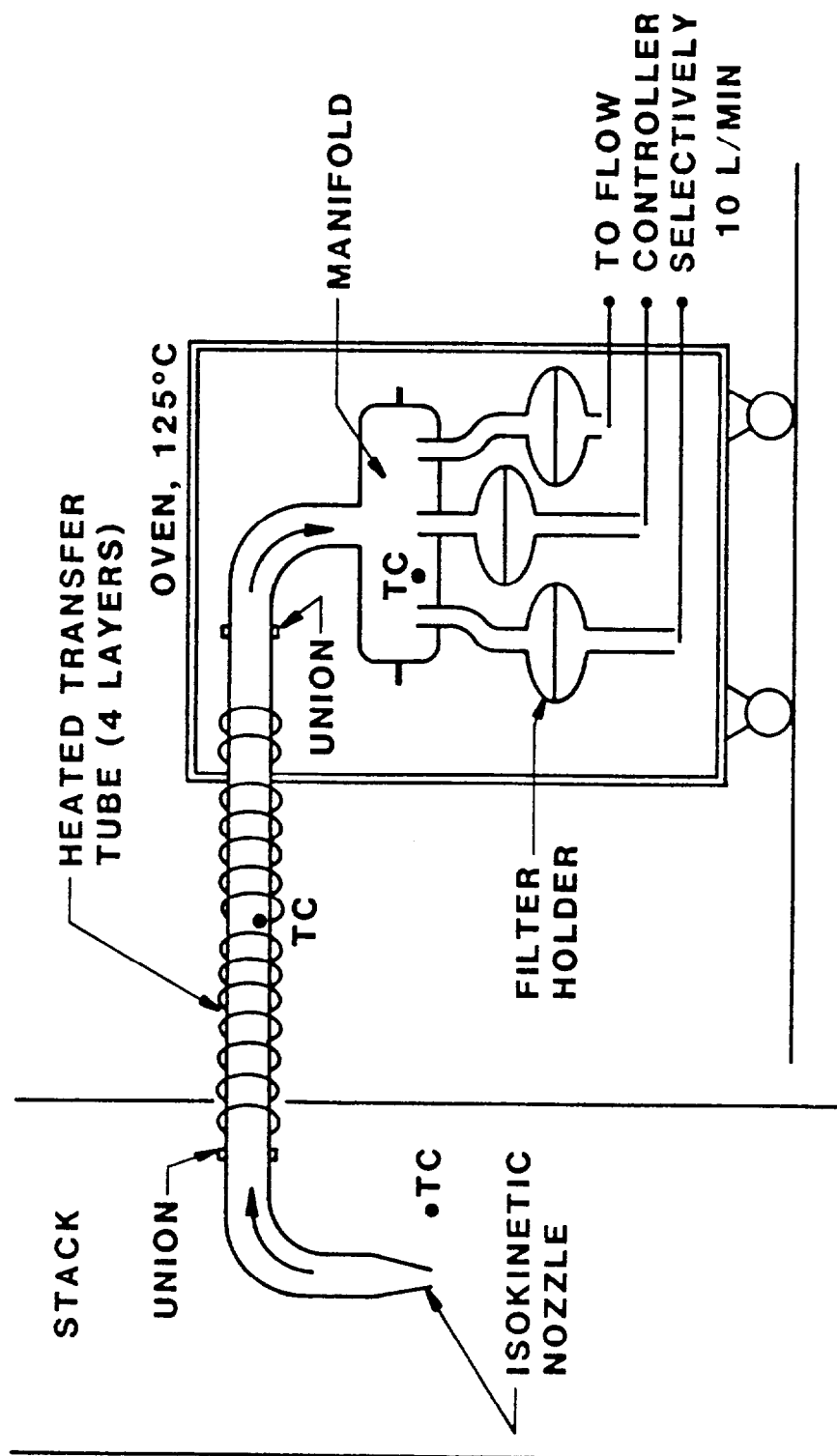FIGURE 1.   INSTRUMENT HOOD FOR OIL BURN EXPERIMENTS

FIGURE 2. 3-FILTER, ALL GLASS, SMOKE COLLECTION SYSTEM

and ease in cleaning. The transmittance of a He-Ne laser, λ = 633 nm, through the smoke in the stack, 0.48 m pathlength, was monitored with a photometer and ratioed to the incident laser intensity to compensate for variations in the source intensity. The design of the photometer is reported by Babrauskas [5]. The laser beam is located about 1 m above the sampling probes. The optics are purged with room air to avoid smoke deposition on the lenses during a test. The uncorrected optical densities (OD's) derived from the transmittance measurements agreed to within 5% with the values of neutral density filters. The OD's of the smoke aerosols were in the range 0.3-1.5. The transmittance measurement is essentially instantaneous and thus provides an indication of the fluctuation in the smoke concentration in the stack.

The gas sampling probe, pitot tube, and thermocouples are located downstream of the horseshoe section of duct. The gas velocity in the stack was determined from the pitot tube measurement together with the thermocouple reading. The sampled gas was cooled with a dry ice trap to remove water vapor, filtered, and then drawn into the gas analyzers. Non-dispersive infrared detectors are used for monitoring the concentrations of CO and CO_2. This information is used in determining the smoke emission based on the carbon balance method.

Samples for study using a transmission electron microscope (TEM) were obtained by rapidly inserting a carbon coated TEM grid into the stack for a few seconds. The primary collection mechanism under these conditions is thought to be via thermophoresis.

CRUDE OIL SAMPLES

Three different crude oils were obtained for study from supplies at EPA-OHMSETT. These were Murban, Larosa, and Prudhoe Bay North Shore crude oils. Testing performed in this study has been limited to evaluations of the Prudhoe Bay North Shore crude oil.

Samples of Prudhoe Bay North Shore crude oil were burned in both 0.4 m and 0.6 m diameter pans. In both cases the oil was floated on a thermally deep layer of water. Emphasis is given in this report to analysis of the combustion process measured in tests with the larger 0.6 m diameter pool fires. Partial results from each of two 0.4 m and two 0.6 m diameter pool fires are given.

ENERGY RELEASE RATE

Figure 3 shows the history of the energy release rate from one of the 0.6 m diameter pool fires. The energy release rate of the burning oil rises rapidly after ignition and flame spread across the surface to a plateau value of about 180 kw (640 kW/m^2). As seen in Figure 3, the energy release rate remains steady through most of the test, but increases dramatically during the last 30 seconds of the burn when the amount of oil left on the water surface is small. The burning rate during this vigorous combustion increases by more than a factor of two. Radiation levels increase to such an extent that the positions where once it was tolerable to stand and observe the experiment now become too close for human comfort. The sublayer of water under the oil can be seen to be boiling vigorously. This boiling persists even after the flames extinguish. The two burning regimes can be seen in Figure 4, photographs of a 0.4 m diameter pool fire experiment. Energy release rates and thermal radiation from both the 0.4 m and 0.6 m diameter pool fires are quantified in
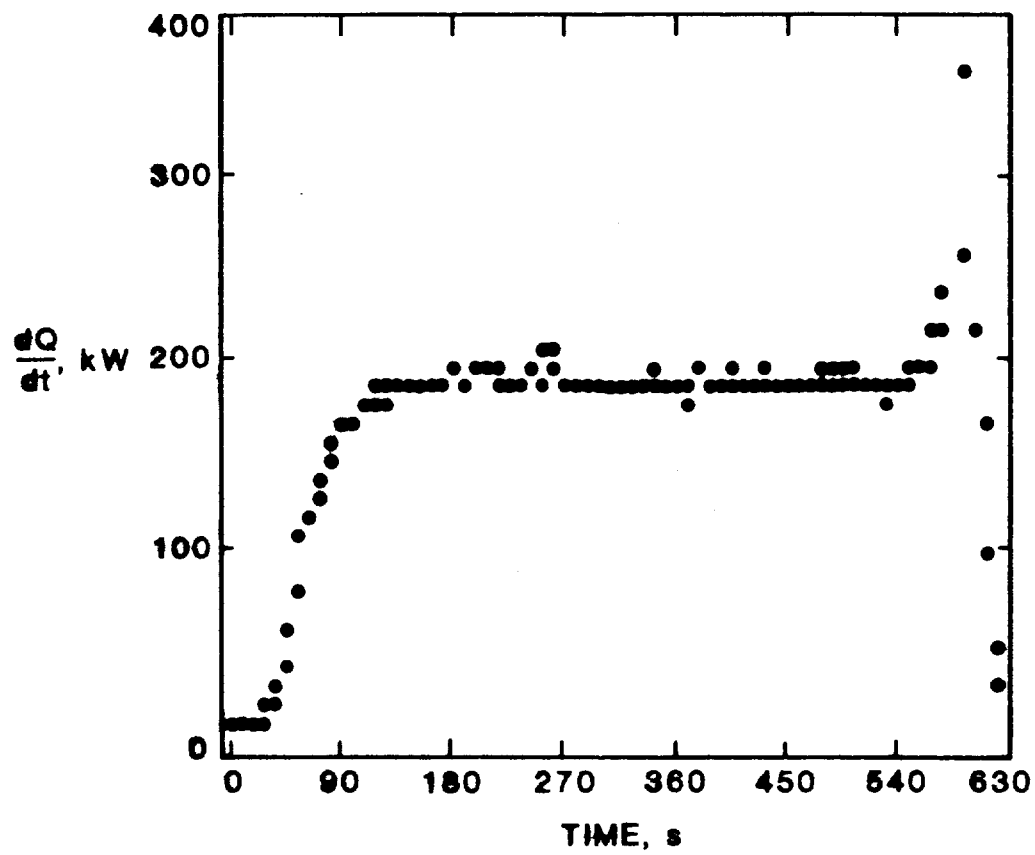
FIGURE 3.   RATE OF ENERGY RELEASE FOR PRUDHOE BAY CRUDE
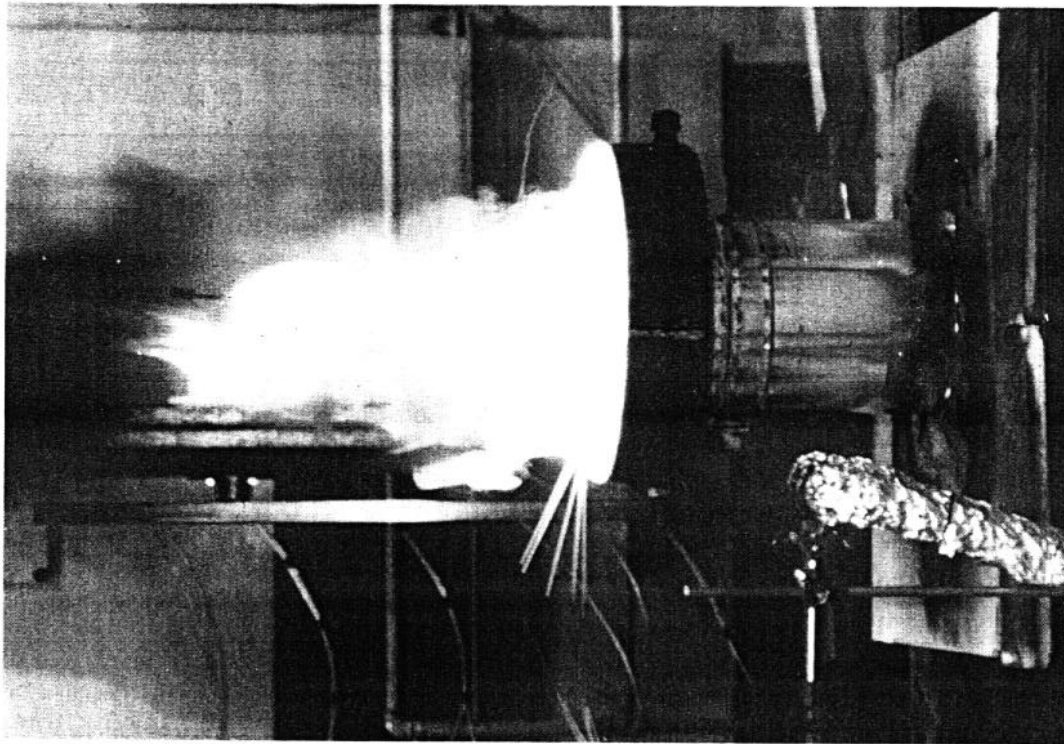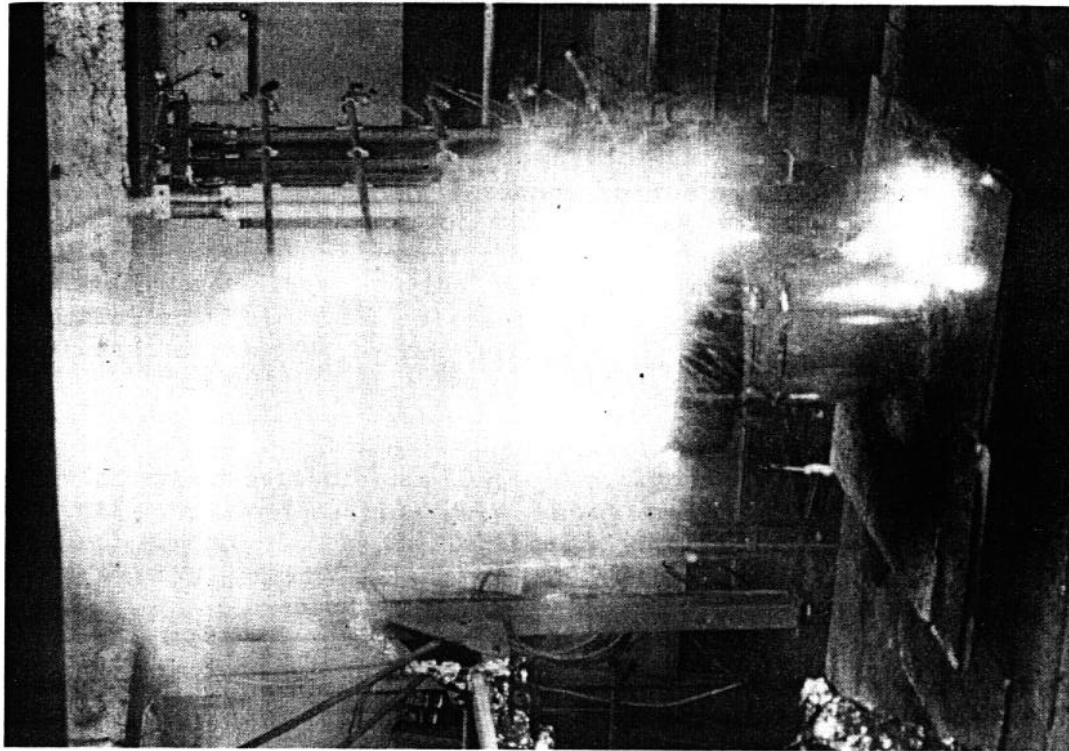OIL BURNED IN A 0.4 METER DIAMETER POOL.

FIGURE 4. PRUDHOE BAY CRUDE OIL FIRE IN 0.4 METER DIAMETER PAN (LEFT) STEADY BURNING (RIGHT) VIGOROUS BURNING AT THE END OF THE TEST
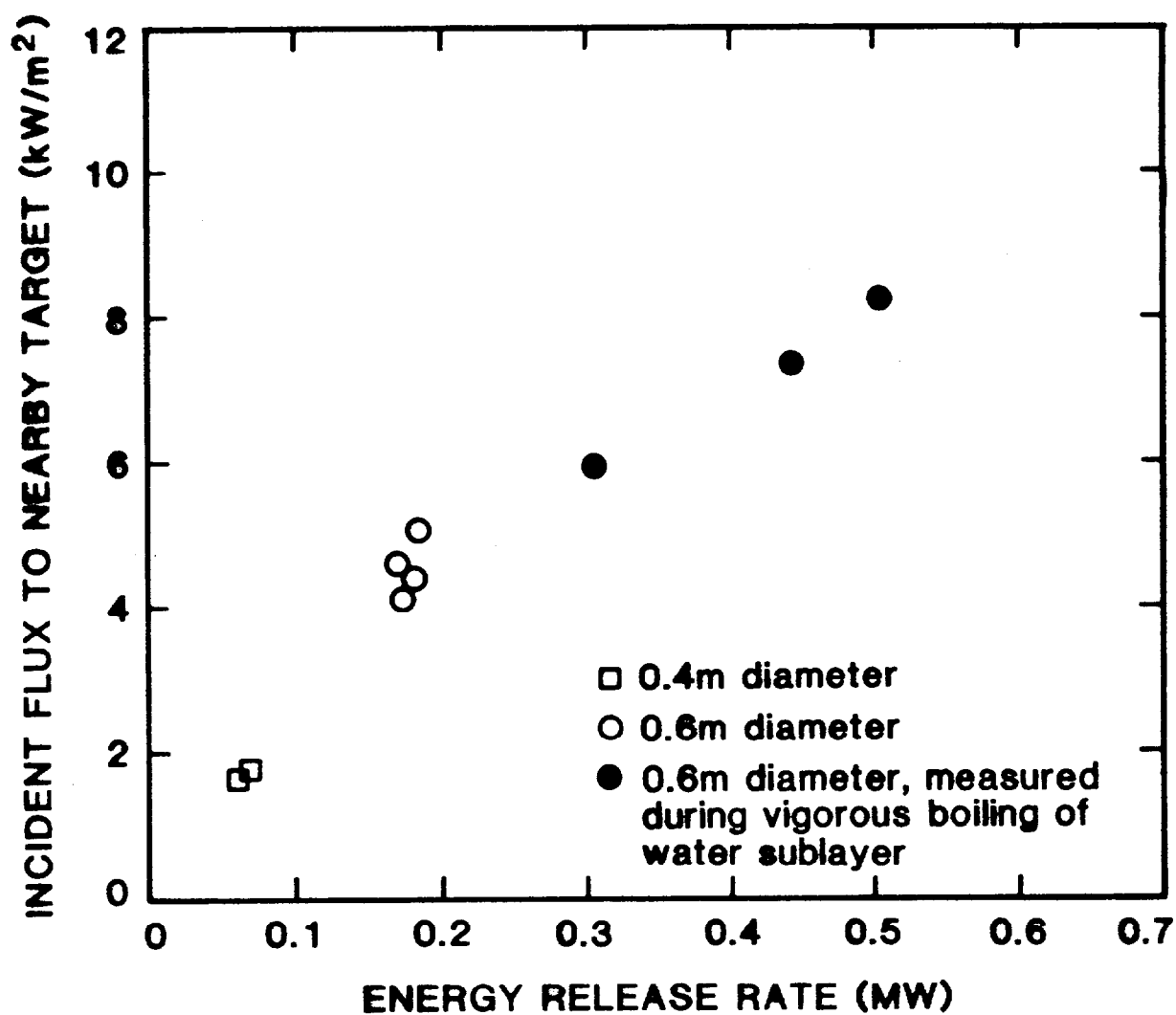
FIGURE 5. RADIATION AND ENERGY RELEASE RATE FROM PRUDHOE BAY CRUDE OIL POOL FIRES.

Figure 5 for both the steady burning period (open symbols) and the vigorous but short burning period before flame extinction (filled symbols). The largest energy release rate measured for the 0.6 m diameter pan was 0.5 MW (1800 kW/m^2) during the vigorous burning period. This vigorous burning period appears as the oil layer becomes thin and sufficient energy from the hot surface and flame causes the supporting water layer to boil. The erupting surface lifts droplets of oil into the flame accelerating the burning process and increasing the energy feedback to the water sublayer which enhances the boiling. Quantification of this process will be part of studies underway involving temperature measurements with rakes of thermocouples immersed in the oil and water layer during burning. The partitioning of energy and its relation to film thickness are important characteristics of the oil combustion process that need to be understood.

SMOKE MEASUREMENT

The smoke aerosol sampling techniques used in this study are suitable to quantify smoke production only during the nominally steady state burning of the oil and not during the relatively short transient period at the end of the burn when vigorous boiling of the water sublayer increases the combustion rate.

Qualitatively there are indications that the smoke aerosol produced during this intense burning contained a tarry component soluble in toluene, in addition to the low density, sooty particles produced during the steady state combustion. A tarry residue was observed on both the impactor and filter nozzles which extend into the exhaust duct. Apparently this resulted from tarry droplets generated during the intense burning impacting on the nozzles. In one experiment, a tarry residue was observed within the impactor, and this was the one experiment in which smoke from the intense burning at the end of the fire was collected. Further discussion of smoke production will be limited to analysis of the steady burning period.

Light Extinction

The light extinction K is related to the light transmittance, I/I_o, via Bouguer's law,

$$I/I_o = e^{-KL},$$
(1)

where L is the path length in meters. As seen in Figure 6, the value of K has a large variability around a fairly constant mean value of about 2 m^{-1}. This large variability is a result of the pulsating characteristic of buoyant plumes in which puffs of smoke can be seen arising from the flame at a frequency of a few Hz. The other instruments, including the gas analyzers and thermocouples, have response times of several seconds and thus do not pick up this pulsation.

In addition to the extinction coefficient, there are two reduced extinction coefficients of interest. The first is K_s, the extinction coefficient per mass concentration of smoke, m_s

$$K_s = K/m_s$$
(2)

The quantity K_s is an intrinsic property of the smoke depending on the wavelength of light, the optical properties of the smoke, and the size distribu-
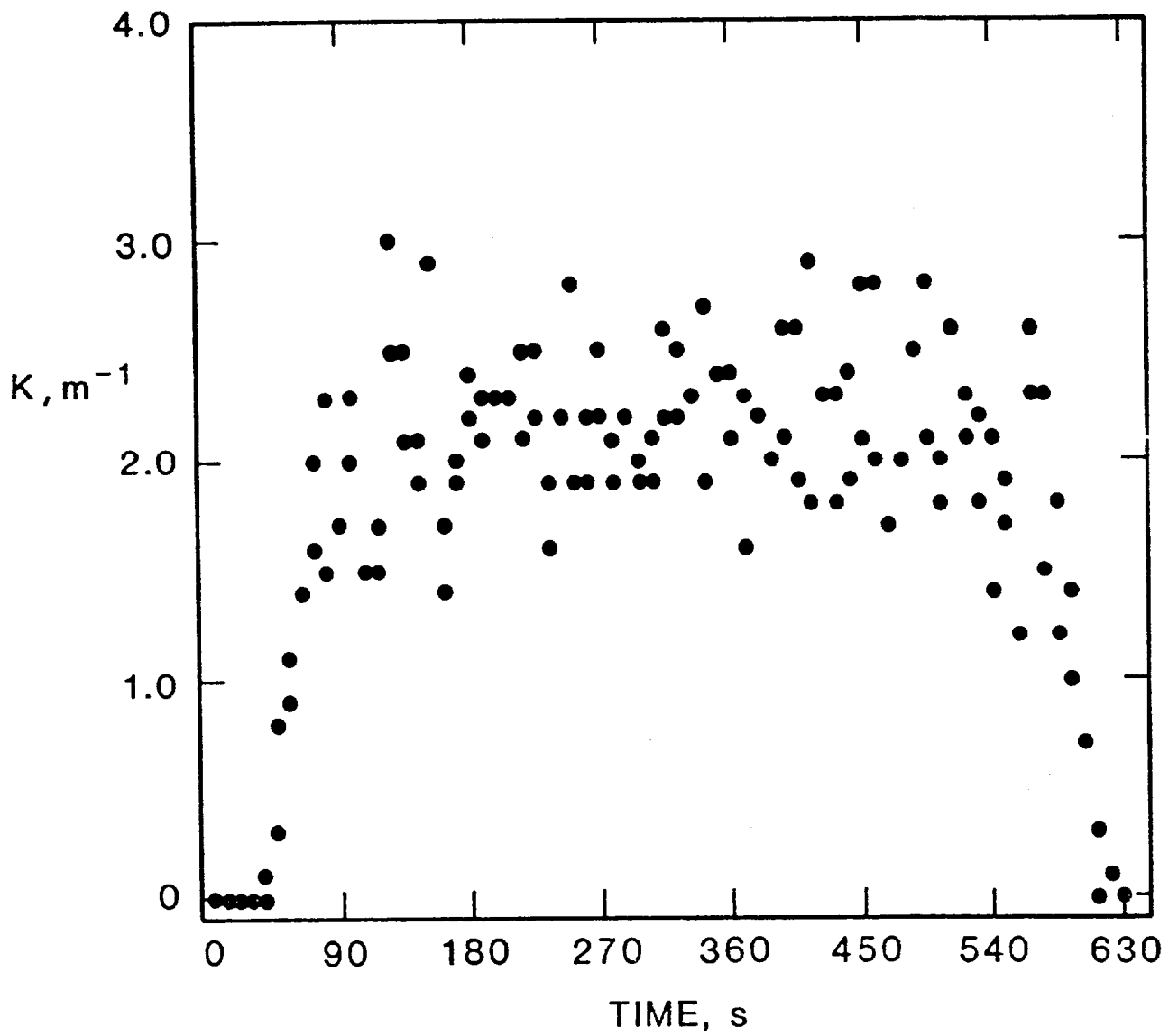
FIGURE 6.   LIGHT EXTINCTION COEFFICIENT FOR PRUDHOE BAY CRUDE
            BURNED IN 0.6 METER DIAMETER POOL.

tion of smoke. As indicated in Table 1, K_s is relatively constant during the burn and has a mean value of 8.8 m^2/g. This is to be compared to Seader and Einhorn's [6] value of 7.6 m^2/g obtained from smoke produced during the flaming combustion for a variety of fuels including wood and plastics. Some difference in the results is expected since Seader uses a white light source while a monochromatic source with $\lambda = 633$ nm is used in this study.

The second reduced extinction coefficient, K_f, is the extinction coefficient per unit mass loss concentration,

$$K_f = K/(dm/dt/dv/dt) \tag{3}$$

where dm/dt is the sample mass loss and dv/dt is the volumetric flow rate of gas up the stack. One advantage of this quantity is that a measurement of the smoke concentration is not required. The plot of K_f in Figure 7 suggests that there is a gradual increase in K_f with respect to time. This trend may result from the higher vapor pressure paraffin component of the fuel burning preferentially early in the test with a lower soot yield while the higher sooting aromatic and asphaltene components burn at the later stage.

Smoke Emission

Two methods were used for determining the smoke conversion factor ε, which is defined by

$$\varepsilon = \text{mass of smoke aerosol produced/mass of fuel burned}$$

The first method, termed the flux method, is based on the measurement of the smoke collected on the filter, m_s, and on the mass loss of the sample, m_L, over the same time period. The factor ϕ, which equals the ratio of the mass flow of air up the stack to the mass flow to the filter, accounts for the small fraction of the total smoke yield sampled.

$$\varepsilon_1 = \left(m_s/m_L\right)\phi \tag{4}$$

The second method is the carbon balance method, which is based on the measurement of CO_2, CO, and smoke aerosol. These represent the major carbon containing products of combustion for free burning. The concentrations of CO_2 and CO are relatively constant throughout the tests as shown in Figure 8. The CO_2 concentration in the stack, minus the background concentration equals 0.55% by volume which is a factor of 15 greater than the CO concentration. The mass concentration of carbon in the form of CO_2, M_c (CO_2), is obtained from the volume fraction of CO_2, F_{CO_2}, with background subtracted, via the formula

$$M_c (CO_2) = F_{CO_2} \, \rho_{CO_2} \, (12/44) \tag{5}$$

The factor (12/44) accounts for the carbon mass fraction of CO_2 and ρCO_2 refers to the density of CO_2 within the instrument. A similar expression is obtained for M_c (CO). The mass fraction of carbon in the smoke aerosol is given by

$$f_s = M_s/\left(M_s + M_c (CO_2) + M_c(CO)\right) \tag{6}$$

TABLE 1. SMOKE EMISSION AND PROPERTIES FOR 60 CM DIAMETER
PRUDHOE CRUDE POOL FIRE TEST NW35

Property	Sample 1, 30 sec.[a] after ignition	Sample 2, 230 sec. after ignition	Sample 3, 335 sec. after ignition
dQ/dt, kW	153	186	181
ε_2	0.72×10^{-1}	0.80×10^{-1}	0.87×10^{-1}
F_{CO_2}, Vol. fraction[b]	0.46×10^{-2}	0.55×10^{-2}	0.54×10^{-2}
F_{CO}, Vol. fraction	0.26×10^{-3}	0.34×10^{-3}	0.36×10^{-3}
K_s, m^2/g	9.30	8.84	8.25
M_s, g/ℓ^3 [c]	0.217×10^{-3}	0.293×10^{-3}	0.312×10^{-3}

[a]The filter samples are collected for 1 minute and the properties listed in column 1 are averaged over this time interval.

[b]The background CO_2 concentration has been subtracted.

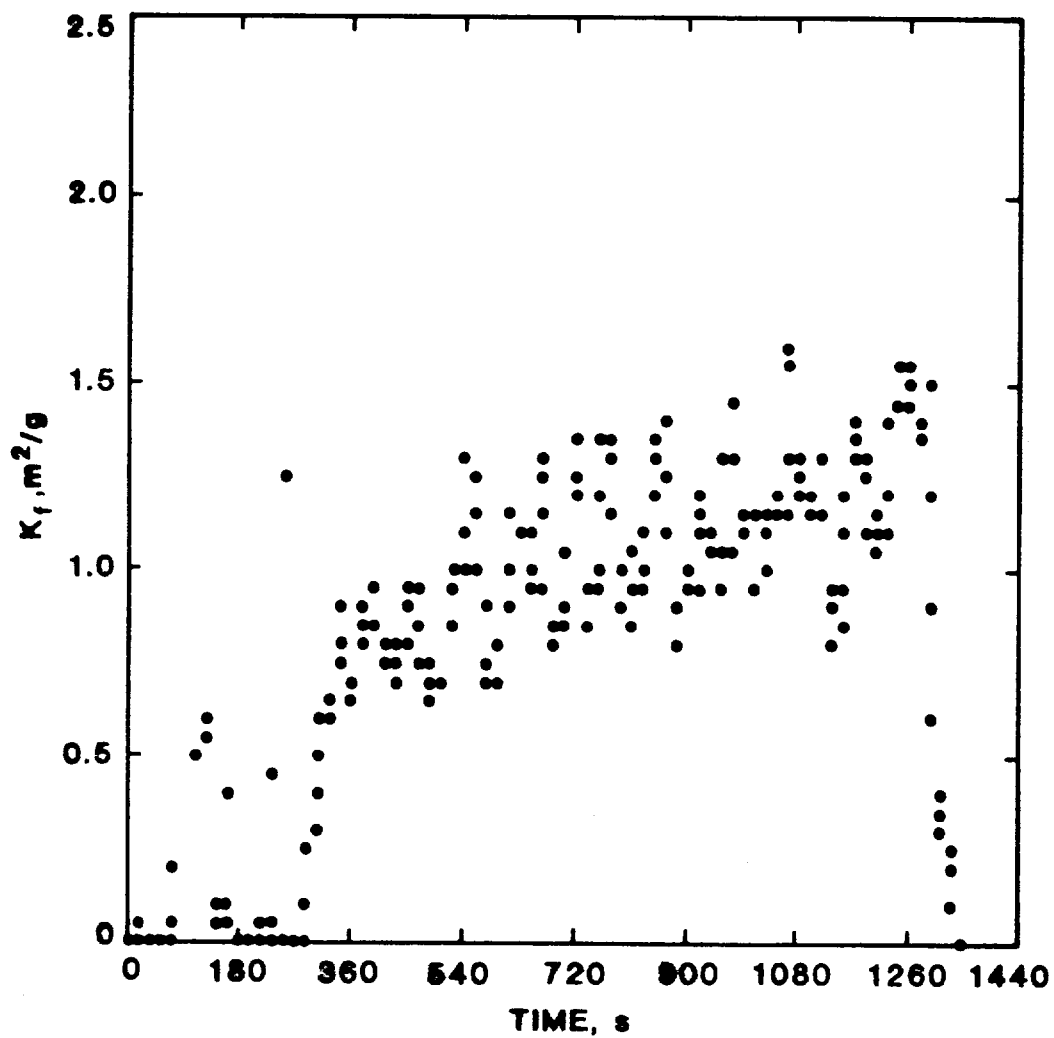[c]Smoke concentration corrected to ambient conditions.

FIGURE 7.   SPECIFIC EXTINCTION COEFFICIENT RELATIVE TO FUEL
FOR PRUDHOE BAY CRUDE OIL BURNED IN A 0.4 METER
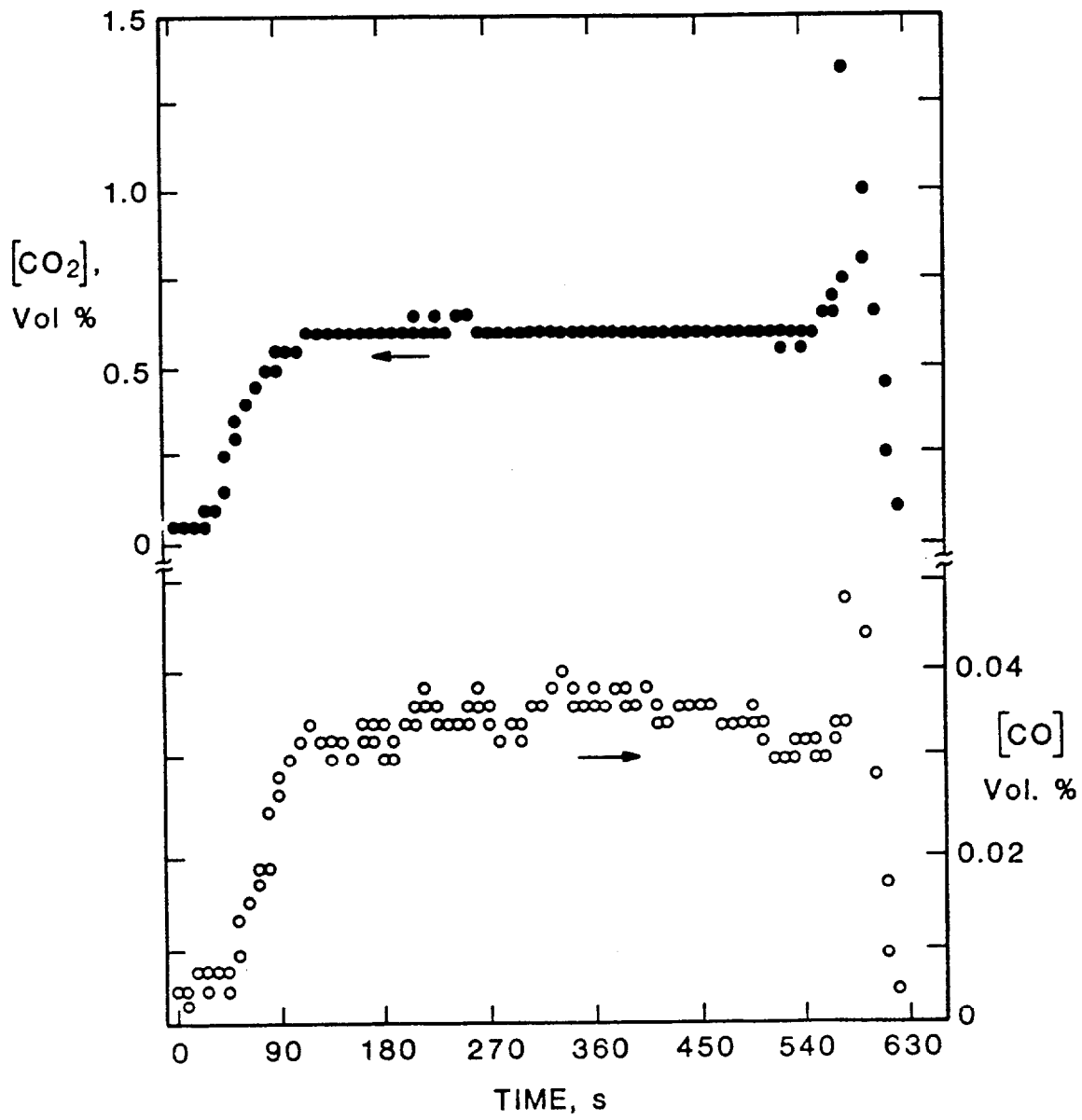DIAMETER POOL.

FIGURE 8. CO_2 AND CO CONCENTRATIONS FOR PRUDHOE BAY CRUDE OIL BURNED
IN 0.6 METER DIAMETER POOL.

Finally, we obtain ε_2 by multiplying F_s by the carbon mass fraction of the fuel, F_c.

$$\varepsilon_2 = f_s F_c \tag{7}$$

Lacking data on F_c for Prudhoe Bay crude oil, we have taken F_c to be 0.86, which is at the upper range for elemental carbon in crude oils. A slight overestimate is obtained in this analysis since the smoke is assumed to be 100% carbon. One might also expect a slight contribution from the hydrocarbon gases. Overall, we expect that these approximation will affect the final result by less than 5%.

As an example, for Sample 1 from Test NW35 (Table 1), we calculate the mass fraction of carbon in the form of CO_2, CO, and smoke aerosol. First eq. (5) is used to calculate the mass concentration of carbon corresponding to the volume fractions F_{CO_2} and F_{CO} in Table 1. The density of CO_2 and CO under test conditions is computed from the ideal gas law as:

$$\rho_{CO_2} = \frac{44P}{RT} \; ; \; \rho_{CO} = \frac{28P}{RT} \tag{8}$$

For Test NW35 (Table 1) P = 0.976 atmospheres, and T = 295 K. The appropriate gas constant R is 0.082 liter-atm/gmole/K. The mass fraction of carbon in the smoke aerosol is obtained from eq. (6). The mass fractions of CO_2 and CO are also obtained from eq. (6) with M_s in the numerator replaced by M_c (CO_2) and M_c (CO), respectively. The results are 0.867 of carbon in the form of CO_2, 0.049 as CO and 0.084 as smoke aerosol.

Size Distribution

Samples collected from the seven stages and backup filter of the cascade impactor are shown in Figure 9. The first impaction stage is a single relatively low velocity nozzle, which impacts out particles with aerodynamic diameters greater than 13 μm. With each successive stage, smaller and smaller particles are impacted out as indicated by the particle size cutoffs in Figure 9. The fact that the size distribution is very wide is indicated by the smoke aerosol deposition on each stage.

The quantitative results regarding the size distribution function are shown in Figure 10. The cummulative aerodynamic size distributions are plotted for data obtained from two 60 cm Prudhoe Bay crude oil burns. In both cases, about 20 mg of smoke aerosol were collected on the impaction stages plus backup filter. Since the plot in Figure 10 is on log-probability paper, the straightline fit to the data indicates that the mass distribution is log-normal. The mass median diameter, the 50% point in terms of mass, is found to be 0.5 μm for both experiments. The geometric standard deviation, σ_g, for the size distribution is obtained from the relation

$$\sigma_g = D \, (84.1\%)/D \, (50\%) \tag{9}$$

We find σ_g equal 7.1 and 6.4 for the 60 cm pool burns on test number NW35 and test number NW36, respectively. For a log-normal distribution [7] 67% of the aerosol mass is in the particle diameter range log D_{50} ± by σ_g; for D_{50} = 0.50 μm and σ_g = 7.1, this corresponds to the size range 0.07-3.55 μm. This represents a very broad size distribution.

The complexity of the particle structure is indicated by the transmission electron micrographs in Figures 11 and 12. It is seen that the particles have

TABLE 2. SUMMARY OF SMOKE EMISSION DATA FOR 40 AND 60 CM DIAMETER
PRUDHOE CRUDE POOL FIRES

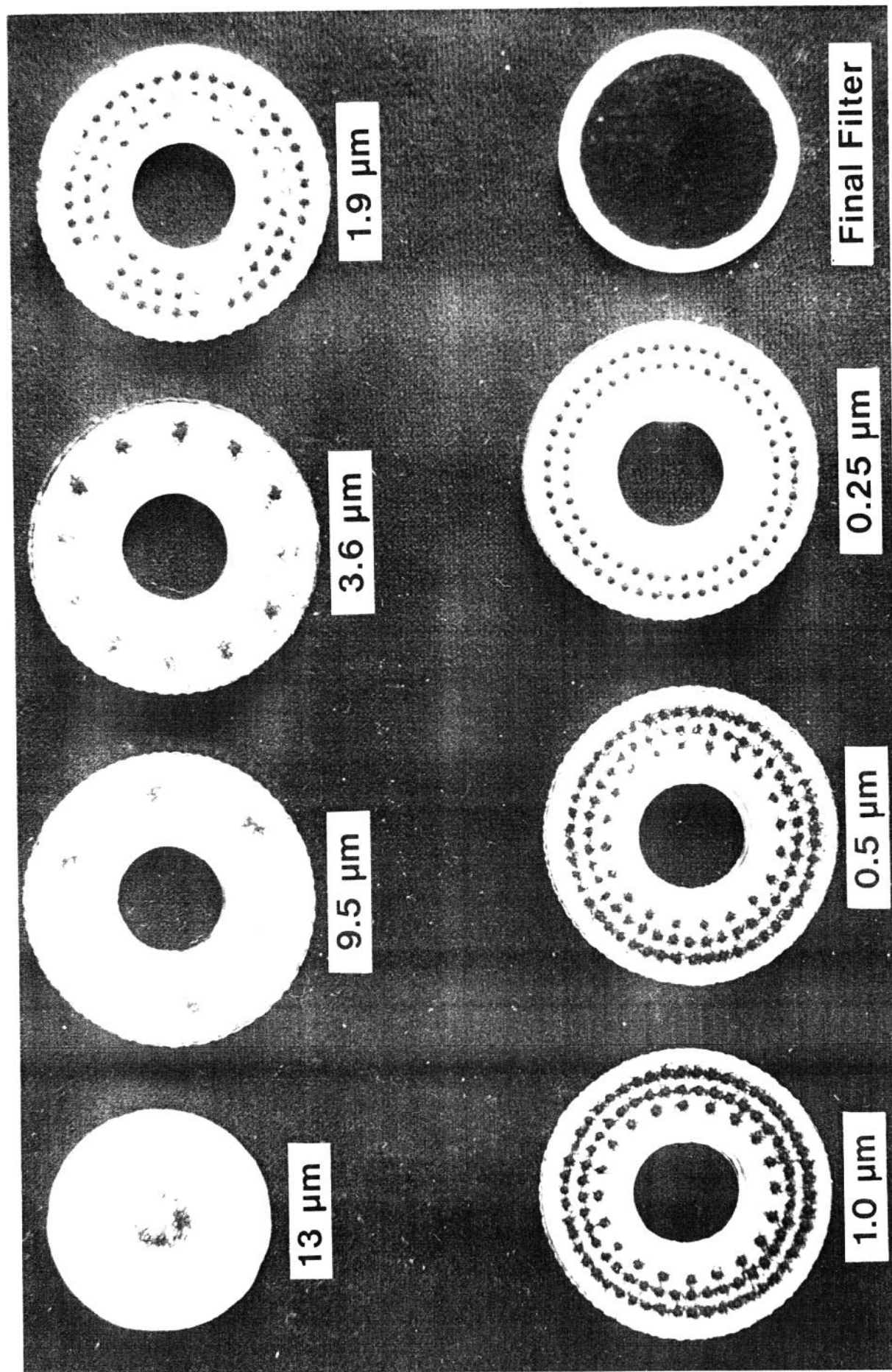| Property	Test NW33 40 cm pool	Test NW34 40 cm pool	Test NW35 60 cm pool	Test NW36 60 cm pool	Average
dQ/dt, kW	63	61	173	178	
dm/dt, g/s	1.81	1.75	–	–	
ε_1	0.107	0.096	–	–	
ε_2	0.098	0.079	0.080	0.090	0.087 ± 0.009
F_{CO_2}, Vol. fraction	0.15×10^{-2}	0.18×10^{-2}	0.52×10^{-2}	0.53×10^{-2}	
F_{CO}, Vol. fraction	–	–	0.32×10^{-3}	0.32×10^{-3}	
K_s, m^2/g	8.95	10.00	8.80	8.64	9.10 ± 0.61
K_f, m^2/g	0.96	0.96	–	–	
D_m, μm	0.74	0.62	0.50	0.50	
σ	5.8	6.4	7.1	6.4	

FIGURE 9. SMOKE AEROSOL DEPOSITION ON SEVEN STAGES AND BACKUP FILTER OF CASCADE IMPACTOR FROM 0.6 METER DIAMETER PRUDHOE BAY CRUDE OIL POOL FIRE.
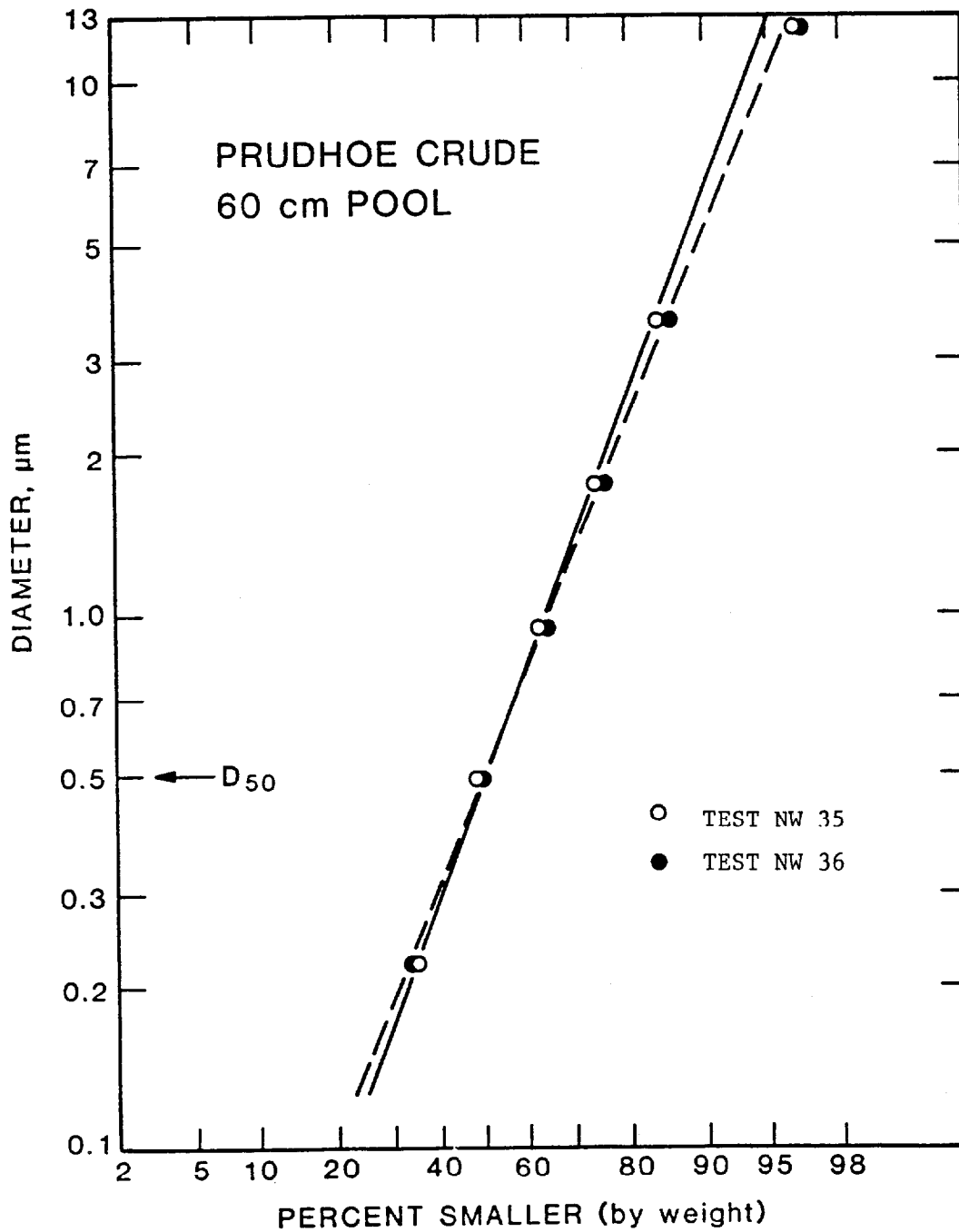
FIGURE 10. CUMMULATIVE AERODYNAMIC SIZE DISTRIBUTION OF SMOKE AEROSOL
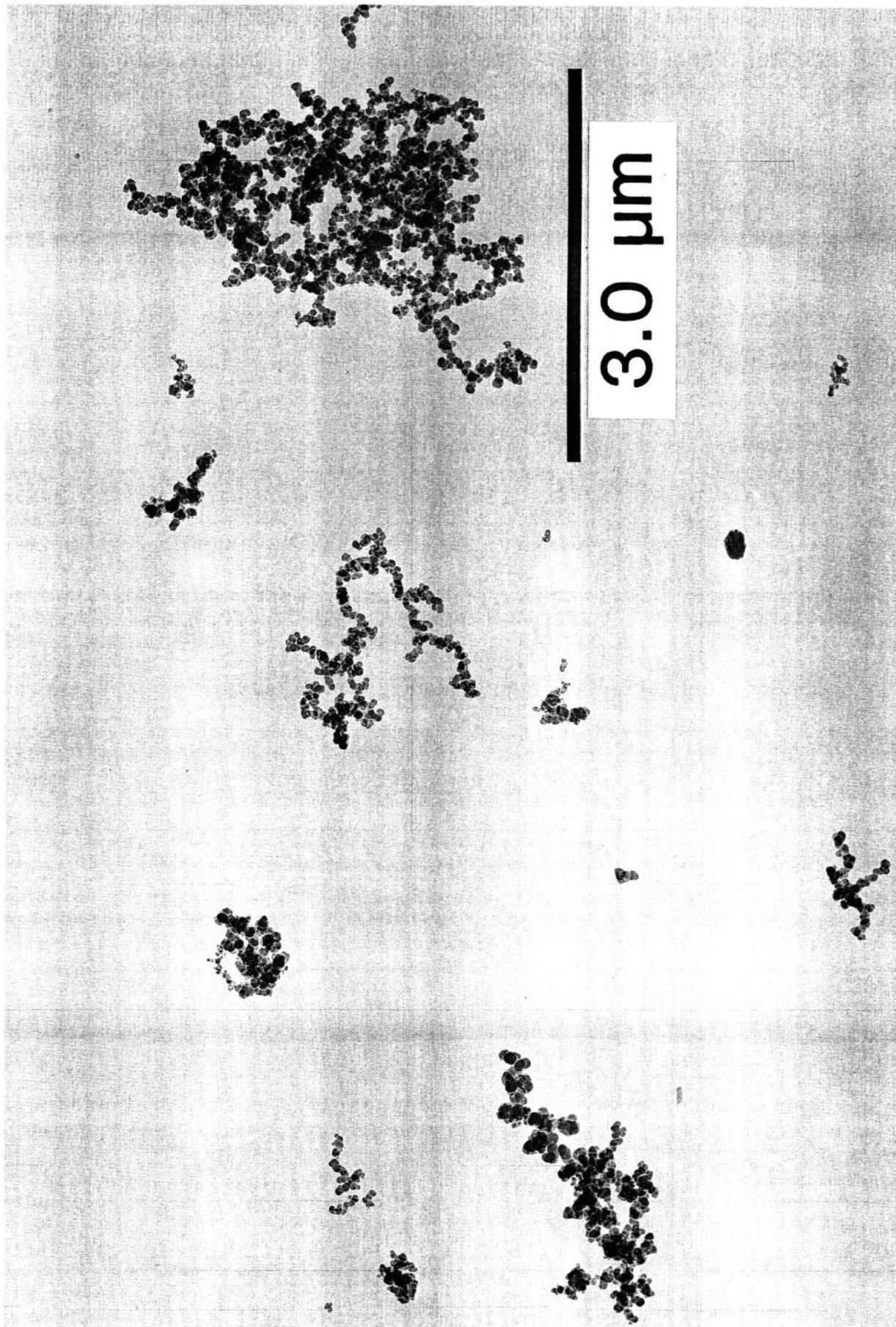PRODUCED BY 0.6 METER DIAMETER PRUDHOE BAY CRUDE OIL POOL FIRE.

FIGURE 11. ELECTRON MICROGRAPH OF SMOKE PARTICLES PRODUCED BY 0.6 METER DIAMETER PRUDHOE BAY CRUDE OIL POOL FIRE, 3 MICROMETER SCALE.
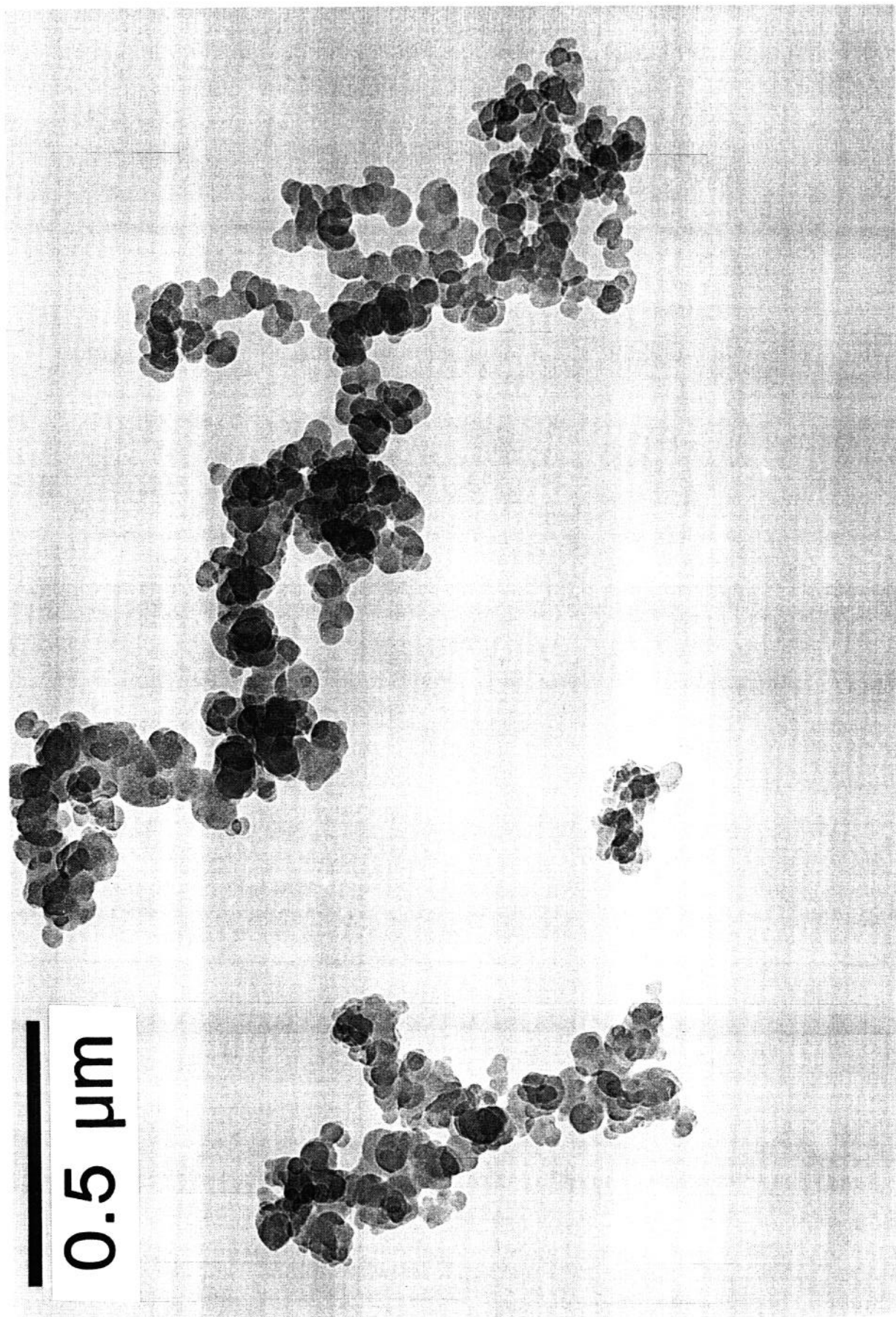
FIGURE 12. ELECTRON MICROGRAPH OF SMOKE PARTICLES PRODUCED BY 0.6 METER DIAMETER PRUDHOE BAY CRUDE OIL POOL FIRE, 0.5 MICROMETER SCALE.

0.5 μm

a low density agglomerate structure made up of many small spherules in the size range 0.02-0.06 μm. As is apparent from Figure 11, there is a wide range in cluster size.

Discussion

A summary of the results from four pool burns is given in Table 2. Increasing the pool size from 40 to 60 cm more than doubles the heat release rate and the mass loss rate of fuel, but it has a relatively minor effect on the smoke conversion factor and in the smoke properties. The emission of smoke is high with ε about 0.10 (10% conversion to smoke) and the specific extinction coefficient, $K_s = 9.1$, is similar to what has been observed for other soot producing fuels. Over 50% of the smoke aerosol is in the submicrometer aerodynamic size range, which is indicative of a long atmospheric residence time and potentially high deposition in the lower respiratory tract.

One of the most striking features of the burning oil is the very rapid combustion over the final thirty seconds. There are qualitative indications that the smoke aerosol produced under these conditions has a significant tarry component not seen in the smoke collected during the steady combustion phase. This is potentially an important effect since the thickness of the oil layer resulting from a spill may be relatively small compared to the initial thickness in the test fires of 0.27 m. A significant fraction of the total smoke emitted from combustion of an oil spill originate from the intense burning phase.

The fact that we do not see any significant scale effect in regard to smoke emission may simply be a result of the relatively narrow range of scales studied. An increase by a factor of 10 to 100 in burning rate may have a significant effect on the smoke aerosol emission and smoke properties.

The smoke aerosol collection and characterization has been carried out at elevated temperatures around 100°C. Without further study, one can not be certain whether the results are directly applicable to diluted, aged smoke aerosol that would be characteristic of smoke far downwind of actual fires.

BURN RESIDUE COMPOSITION

The burning effects on the composition of Prudhoe Bay crude oil was examined by comparative ^{13}C NMR spectroscopy [8] between fresh oil and the burn residue. Of specific interest was the fate of the lighter fractions, which include the short-chain alkanes, cycloalkanes, and substituted benzenes.

The ^{13}C NMR spectra were collected at 100 MH$_z$ with proton decoupling and nuclear Overhauser enhancement. Solutions of crude oil and burned crude oil were 50% by volume in deuterochloroform.

The principal peaks in the aliphatic region of the crude oil spectrum are assigned in Figure 13 to either chain-ending carbons (C_1 through C_4) or chain-interior carbons (C_i) in alkanes. Their relative intensities reflect the distribution of alkane chain lengths. Upon burning, the C_1 through C_4 intensities are uniformly attenuated in relationship to the intensity of C_i. This result is interpreted as a selective depletion of short chain alkanes in the burned crude. A similar fate is indicated for the cycloalkanes. Their resonances, which are marked with asterisks (Fig. 13), are either absent from or attenuated in the spectrum of the burned crude. Evidence of burning effects is much more dramatic in the aromatic region (Fig. 14) of the crude oil spectra. The sharp signals in Figure 14, which are due mainly to mono-ring aromatics including benzene, toluene, and xylenes, are for the most part absent in the burned crude spectrum (Fig. 14).
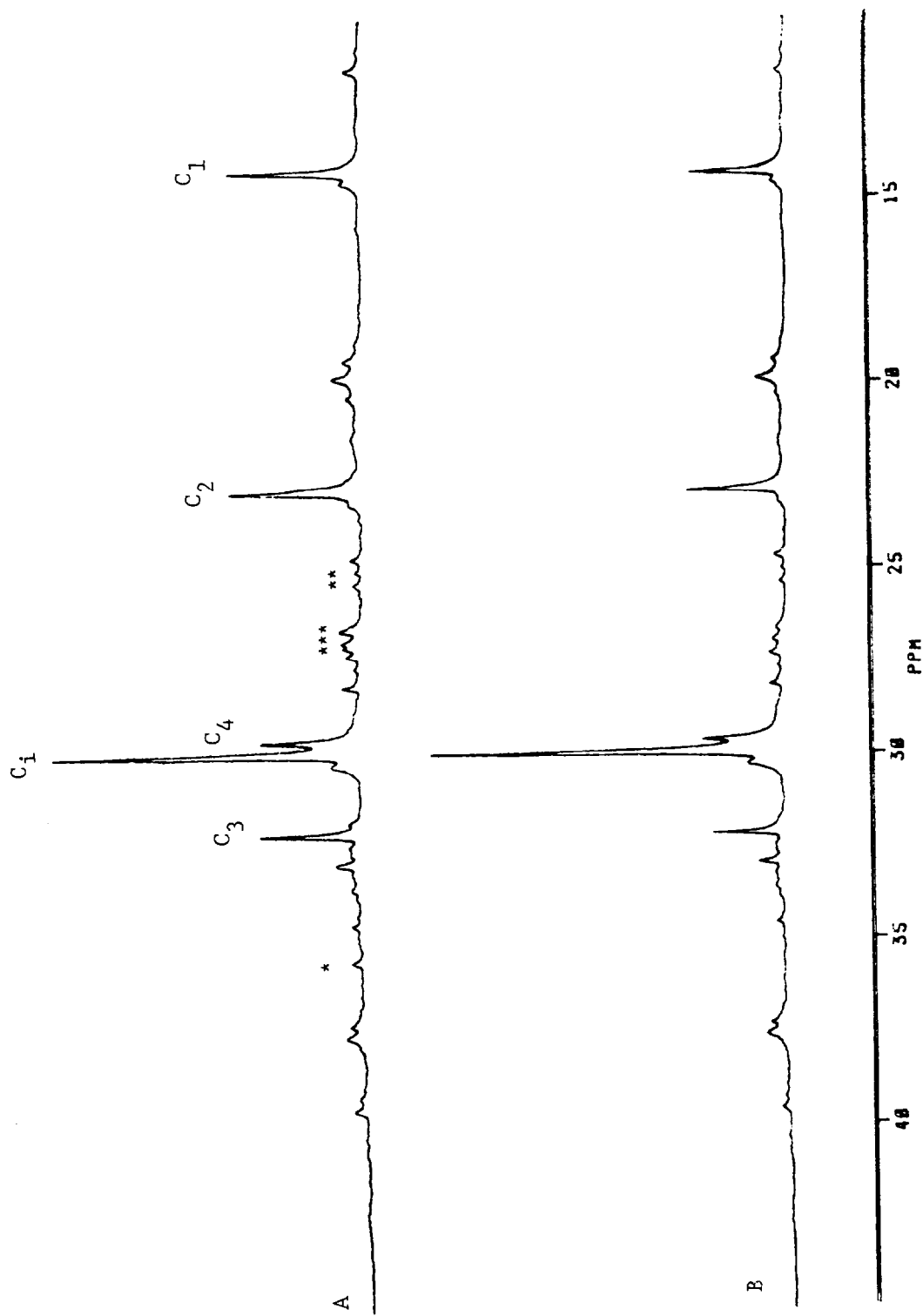
FIGURE 13. A COMPARISON OF THE ALIPHATIC REGION OF THE ^{13}C NMR SPECTRA OF (A) PRUDHOE BAY NORTH SHORE CRUDE OIL, AND (B) BURN RESIDUE OF PRUDHOE BAY NORTH SHORE CRUDE OIL.
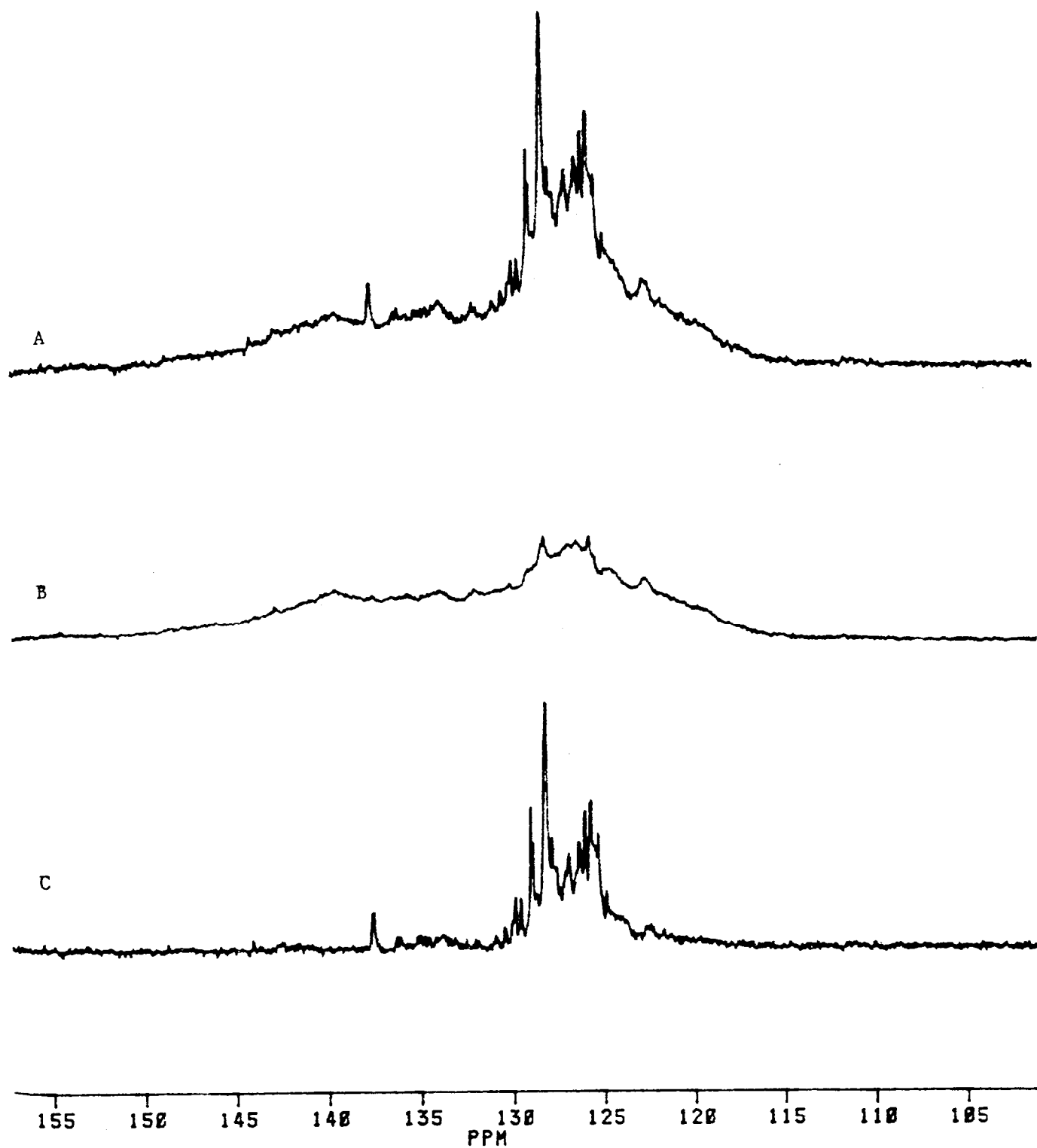
FIGURE 14. A COMPARISON OF THE AROMATIC REGION OF THE ^{13}C NMR SPECTRA OF
(A) PRUDHOE BAY NORTH SHORE CRUDE OIL, (B) BURN RESIDUE OF
PRUDHOE BAY NORTH SHORE CRUDE OIL, AND (C) THE DIFFERENCE
(A-B), BROAD BAN RESONANCES WERE NORMALIZED TO EQUAL INTENSITY.

A more quantitative examination of the depletion of specific alkanes and cycloalkanes would require a combination of gravimetric and ^{13}C NMR analyses of distillation fractions. This type of analysis is being planned.

CALCULATION OF INDUCED AIR FLOW

In recent years there has been an interest in determining if it is possible for fire induced air flows into large fires to cause a migration of the oil spill towards the burning area. Large oil burns on water have been conducted to measure this induced surface air flow [9]. These experiments, although carefully conducted, are hard to interrupt because of non-ideal conditions encountered in field testing such as uncontrolled ambient winds. It is also known, particularly in the case of oil spills, that clean-up will require the ignition of many relatively small patches of oil that are separated by either open water or layers of oil too thin to ignite.

This part of the study details a calculation of induced wind into an area containing randomly distributed fire sources having various steady energy release rates. Present calculations do not include any interaction between the induced flow and the surface. A sample calculation of the induced air flow velocity field 0.8 m above the surface over an area 100 m x 100 m containing 20 fires ranging in energy release rate from 200 kW to 3.2 MW was performed. Based on the measured energy release rate for Prudhoe Bay crude oil in a 0.6 m diameter pool of 640 kW/m^2 these fires would represent crude oil pools ranging in diameter from 0.63 m to 2.5 m.

The Model for Fire Induced Flow

The flow induced by an oil spill fire is primarily determined by three factors: the geometrical arrangement of the burning parcels of fuel, the rate of heat released by each individual fuel element, and the atmospheric environment in the neighborhood of the spill. In any given spill scenario, there is a considerable amount of randomness in each of these factors. The mathematical model described below attempts to deal with this situation by combining random distributions of location and burning rate of the individual patches of fuel with a deterministic, description of the composite flow generated by a given realization of the spill scenario. Each patch of burning oil is assumed to be sufficiently removed from the others so that the buoyant plume of hot gas and smoke rising above the patch evolves independently. Under these circumstances, the composite flow field can be decomposed into a collection of individual flows associated with each plume. The flow pattern associated with a single plume is then analyzed in detail and the results compared with experimental data. The process by which the composite flow is calculated is then outlined; and the induced surface wind for a sample distribution of plumes is displayed.

The starting point is the inviscid equations of fluid mechanics which control the large scale fluid motion of interest. These laws, expressing conservation of mass, momentum, energy, and an equation of state, respectively are:

$$\frac{D\rho}{Dt} + \rho \nabla \cdot \vec{u} = 0$$

$$\rho \frac{D\vec{u}}{Dt} + \nabla \tilde{p} - \left(\rho - \rho_o\right) \vec{g} = 0$$

$$\rho C_p \frac{DT}{Dt} = Q \, (\vec{r},t) \tag{10}$$

$$P_o = \rho RT$$

Here P, ρ, $\vec{u}$, and T are, respectively, the local pressure, density, velocity, and temperature in the gas at position $\vec{r}$ and time t induced by a rate of energy release $Q \, (\vec{r},t)$, The gas has a specific heat C_p and gas constant R, while $\vec{g}$ is the gravitational acceleration. The quantities P_o and ρ_o are sea level ambient pressure and density, while $\tilde{p}$ represents the small perturbation from hydrostatic pressure that drives the motion. All plumes are assumed to evolve in uniform atmosphere at rest far from the plumes. The convective operator D/Dt includes local time dependence:

$$\frac{D}{Dt} \equiv \frac{\partial}{\partial t} + \vec{u} \cdot \nabla$$

It is certainly not feasible to contemplate solving eq. (10) directly. Instead, we make use of two equivalent results. If the first of eq. (10) is multiplied by C_p and added to the third and the equation of state is used, the divergence of the velocity field can be expressed as:

$$\nabla \cdot \vec{u} = Q \, (\vec{r},t)/\rho_o C_p T_o \tag{11}$$

Physically, eq. (11) states that the volumetric expansion rate of any fluid element is proportional to the net rate of heat addition. It is important to note that although the heat is added to the atmosphere only in the vicinity of each patch of burning fuel, eq. (11) is valid everywhere above the surface.

The second result needed is Bjerknes theorem [10]. The fluid vorticity $\vec{\omega}$ is defined in terms of the fluid velocity $\vec{u}$ as:

$$\nabla \times \vec{u} \equiv \vec{\omega} \tag{12}$$

Now consider a closed loop of Lagrangian marked particles moving with the local fluid velocity. The circulation Γ around that closed loop is defined as:

$$\Gamma \equiv \oint_{\ell} \vec{u} \cdot d\vec{r} = \oint \vec{\omega} \cdot \vec{n} dA \tag{13}$$

Here $\vec{n}$ is a unit vector normal to any surface A bounded by the closed loop ℓ of marked particles. The momentum conservation equation, the second of eq. (10), can then by manipulated into the form:

$$\frac{d\Gamma}{dt} = \oint_{\ell} \left\{ \left[\left(\rho - \rho_o\right)/\rho_o\right] \vec{g} - \nabla \tilde{p}/\rho \right\} \cdot d\vec{r} \tag{14}$$

Equation (14) is Bjerknes theorem. Physically, it states that vorticity can be created in a fluid away from a boundary only through the mechanism of density gradients. In the absence of such gradients the circulation around the closed loop, and hence the vorticity contained within the loop, cannot change.

Now consider the history of a fluid element originating from rest far from any of the plumes generated by the oil spill fire. Initially the fluid contained no vorticity, and in its approach to the fire it remains irrotational. As it enters one of the smoke plumes it encounters large density gradients, and an intense vortex field is created. Thus, eq. (12) can be rewritten as:

$$\nabla \times \vec{u} = \vec{\omega}_p (\vec{r}, t) \tag{15}$$

Here, $\vec{\omega}_p$ denotes the vorticity in the plumes. Just as in the case of eq. (11), eq. (15) holds everywhere even though $\vec{\omega}_p$ only involves the velocity gradients inside the plumes.

Two further points should be noted. First, since the right hand sides of eqs. (11) and (15) involve only information inside the plumes, if the plumes remain distinct we can write:

$$Q (\vec{r}, t) = \sum_i Q_i (\vec{r}, t)$$

$$\vec{\omega}_p (\vec{r}, t) = \sum_i \vec{\omega}_{pi} (\vec{r}, t) \tag{16}$$

Here the sum is taken over each individual plume. Thus, a velocity field $\vec{u}_i$ can be associated with each plume, where the velocity field is the solution to

$$\nabla \cdot \vec{u}_i = Q_i / \rho_o C_p T_o$$

$$\nabla \times \vec{u}_i = \vec{\omega}_{pi} \tag{17}$$

Second, these formulae are valid both instantaneously and in a time averaged sense. If time dependent information about the structure of an individual fire plume is available, then it can be used in eq. (17). At present, only time averaged information is available. In either case, the kinematics of a general vector field insures that a knowledge of the divergence and curl of the vector is sufficient to determine it everywhere uniquely.

The physical information available on the time averaged structure of fire plumes has been analyzed by McCaffrey [11]. He notes that there is ample experimental support for a Gaussian radial distribution of the mean vertical velocity in the plume. This can be expressed analytically in the form:

$$u = U(Z) \exp \left\{ - \left[r/R(Z) \right]^2 \right\} \tag{18}$$

Here u is the vertical velocity component, U(Z) its value on the center-line of the axially symmetric plume, and R(Z) the mean plume width. The variable Z is the height above the sea surface and r is the radial distance from the plume centerline. McCaffrey furnishes an analytical correlation of the experimental data for U(Z) and the centerline temperature. By enforcing the

requirement for energy and momentum conservation on average across the plume at each height Z, he is able to infer the mean radius R(Z). Using eq. (18) and the fact that the time average plume is axially symmetric, the vorticity $\vec{\omega}$ can be inferred as:

$$\vec{\omega} = \omega_\phi \vec{\phi}$$

$$\omega_\phi \cong [2U(Z)/R(Z)]\{r/R \exp [-(r/R)^2]\} \tag{19}$$

The quantity $\vec{\phi}$ is a unit vector in the azimuthal direction.

The detailed form of the centerline velocity correlation will be shown below. For the moment, the most important aspect of the correlation is the scaling law implied by the overall conservation of energy in each plume. If Q_i is the total rate of energy release into an individual fire plume, then the velocity field induced by that fire depends on a single length scale D_i, defined as:

$$D_i = \left(\hat{Q}_i/\rho_o C_p T_o \sqrt{g}\right)^{2/5} \tag{20}$$

Moreover, the velocity field $\vec{u}_i$ must be of the form:

$$\vec{u}_i = \left(gD_i\right)^{1/2} \vec{u}_* (\vec{r}_*)$$

$$\vec{r}_* = \vec{r}/D_i \tag{21}$$

Thus, a single dimensionless velocity $\vec{u}_*$ can be calculated from eqs. (17) and (19) which is valid for a fire of any strength. Given the dimensionless result $\vec{u}_*$, the physical velocity field for a given fire strength can be determined from eqs. (20) and (21).

The details of the calculation of the universal dimensionless velocity $\vec{u}_*$ will be omitted here. However, the resulting mean streamline pattern is shown in Figure 15. The flow enters nearly horizontally from the right, then turns abruptly upwards as it enters the plume. The approximate plume boundary is moving slowly to the right, growing nearly linearly with increasing height. The relatively close spacing of the streamlines after they enter the plume indicates the high velocities present in the plume. Figure 16 shows the ground level radial inflow velocity induced by the plume. The inflow velocity has two components. The dotted line denoted $U_r(\psi)$ represents the very strong inflow induced by the vorticity in the plume. The dashed line denoted $U_r(\phi)$ represents a weak outflow due to the volumetric expansion associated with the heat released in the flames at the base of the plume. The solid line is the net radial inflow. The peak value corresponds to a location near the outer edge of the flame zone at the base of the plume.

These results can be checked against experimental data in two stages. Figure 17 shows the calculated centerline vertical velocity, the upper solid line, plotted as a function of height. The lower solid line is the dimensionless centerline correlation developed by McCaffrey, based on measurements of laboratory scale fires. The agreement is quite good; the maximum discrepancy between the two curves is about four percent. The calculated velocity is further broken down into the vorticity and expansion induced components, denoted as before by dotted and dashed lines, respectively. Figure 18 shows the correlation compared with experimental data taken from a variety of large scale pool fires. The velocity correlation is replotted in the middle curve. The data, though relatively sparse, tracks the correlation quite well.
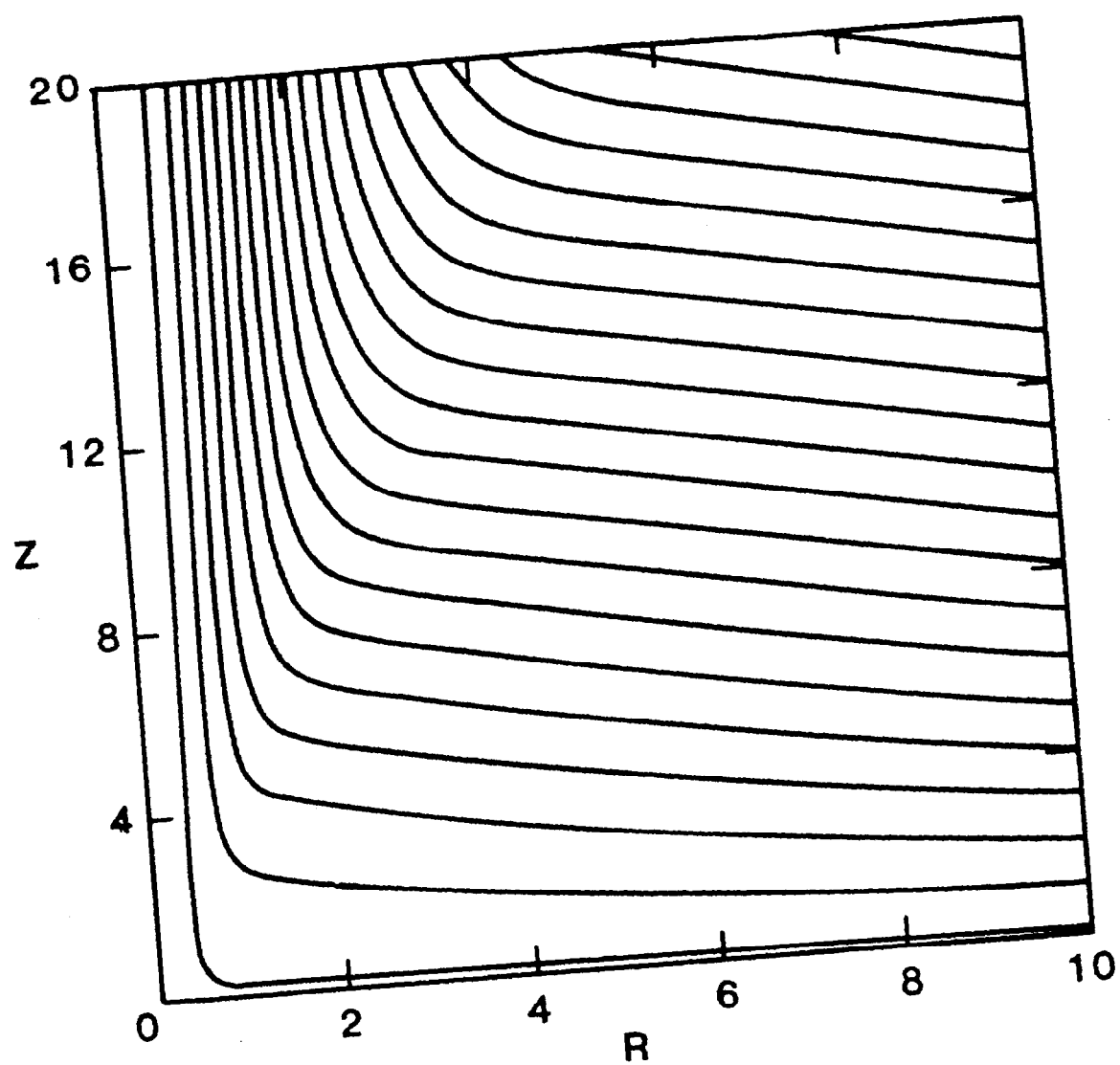
FIGURE 15. TIME AVERAGED STREAMLINES CALCULATED FROM DIMENSIONLESS VELOCITY FIELD IN TERMS OF SCALED RADIAL (R) AND VERTICAL (Z) COORDINATES.
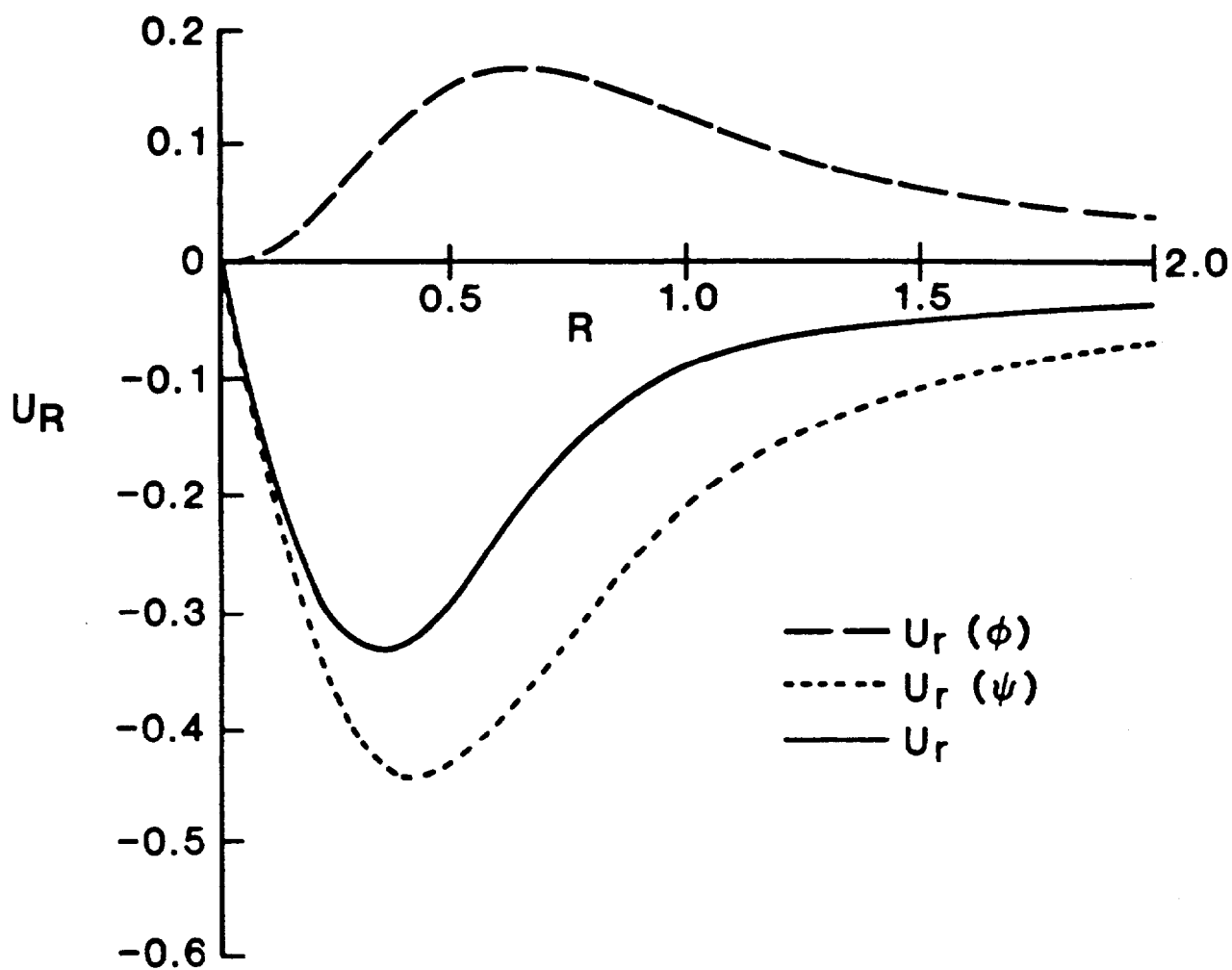
FIGURE 16. GROUND LEVEL RADIAL INFLOW SHOWING VORTICITY INDUCED FLOW U_r (ψ), VOLUMETRIC EXPANSION OUTFLOW U_r (ϕ), AND NET INFLOW U_r.
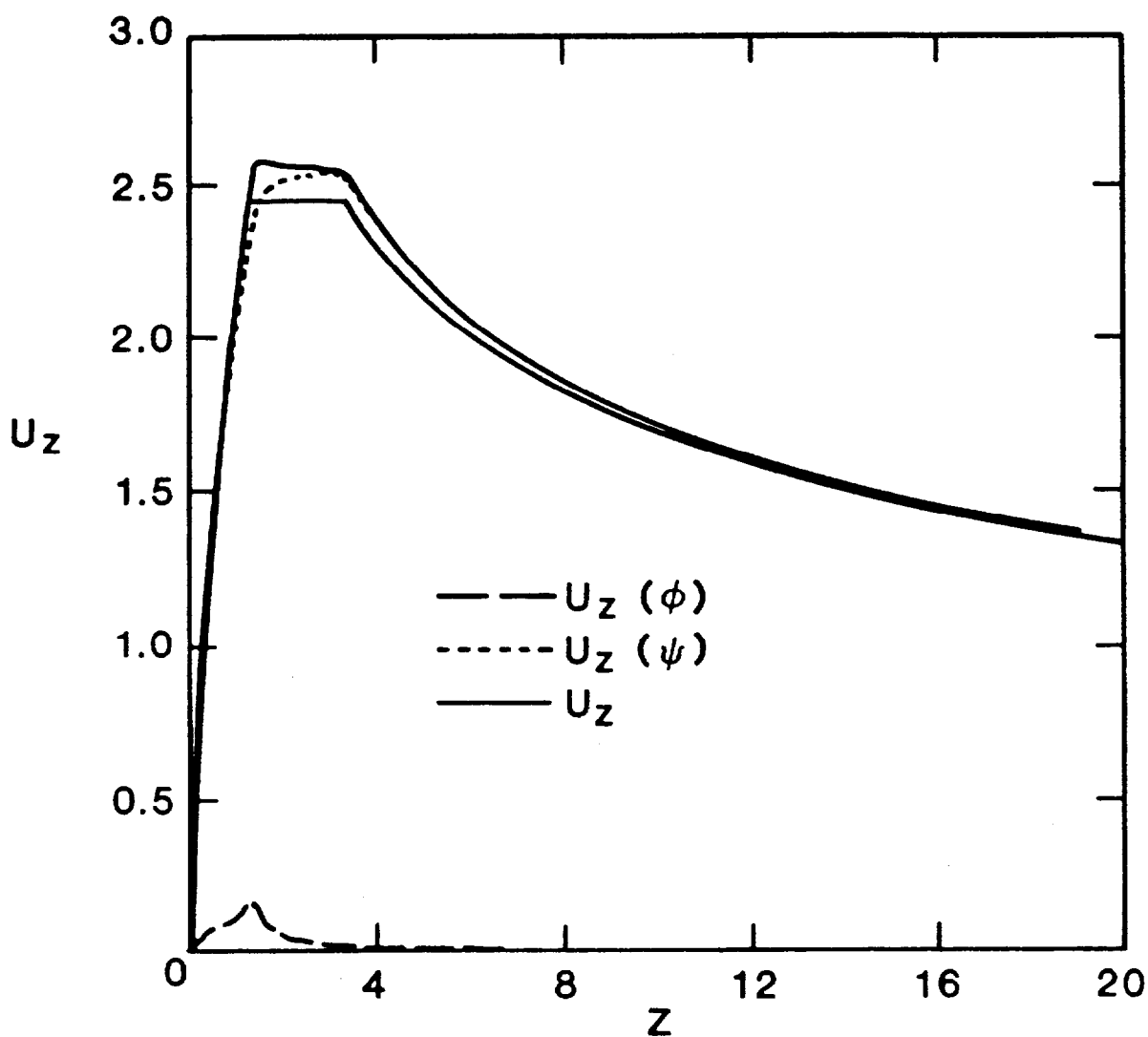
FIGURE 17. VERTICAL PLUME CONTERLINE VELOCITIES SHOWING TOTAL CALCULATED
VELOCITY (UPPER SOLID LINE), DATA CORRELATION (LOWER SOLID LINE),
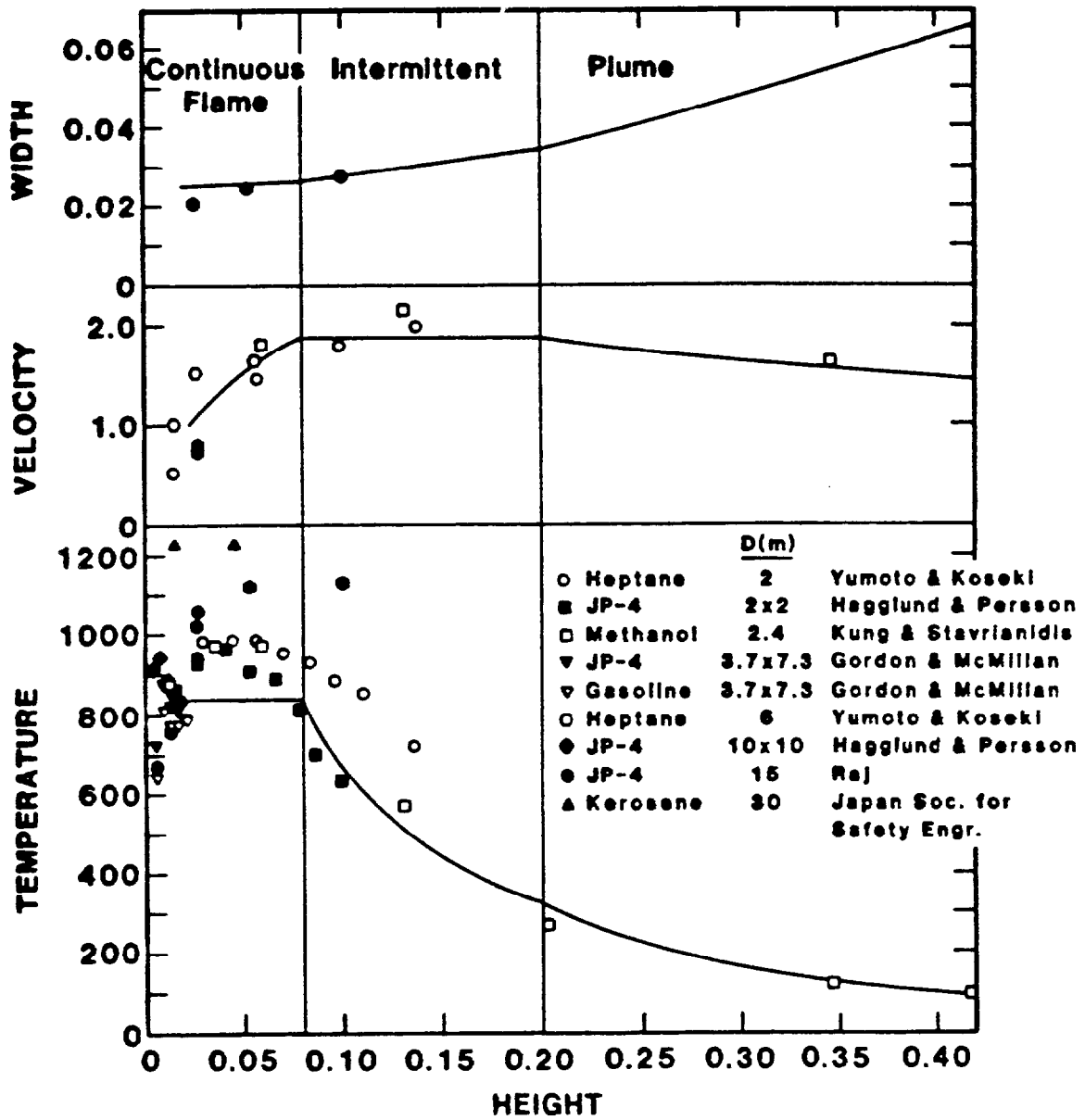VORTICITY INDUCED FLOW U_Z (ψ) AND VOLUMETRIC EXPANSION FLOW
U_Z (ϕ).

FIGURE 18. COMPARISON OF CENTERLINE TEMPERATURE, VELOCITY, AND GAUSSIAN
PLUME WIDTH CORRELATIONS WITH LARGE SCALE POOL FIRE DATA.

Given the non-dimensional solution for the flow induced by a single fire, we now turn to the calculation of the composite flow. The individual plume flow pattern is symmetric about a vertical axis centered above the patch of burning fuel. However, an assemblage of such flows, each with an axis of symmetry in a different location, is inherently three dimensional. Moreover, allowance must be made for the fact that the fires can vary widely in strength. In order to proceed, it is necessary to make some assumptions about location and fire strength. In practice very little information is likely to be available about an oil spill event other than the approximate area covered and the amount of fuel released and burning. Accordingly, a computational scheme is set up which distributes a prescribed number of fires into five discrete strength ranges, each rate of energy release a factor of two larger than that which precedes it. In the absence of any better information, the probability distribution is taken to be uniform with respect to fire strength. Each of the fires is then distributed randomly into an overall rectangular area which is prescribed. The composite velocity near water level is then calculated on a uniform 100 x 100 grid within the spill area.

SAMPLE CALCULATION

A sample calculation is shown in Figure 19. Twenty plumes ranging in strength from 200 kW to 3.2 MW (see Table 3) are randomly introduced into a square 100 meters on a side. Velocity vector arrows of length proportional to the magnitude of the local velocity field are introduced at 5 meter intervals. Contours of constant dimensionless speed are also shown as an aid to locating the burning areas. The areas where the speed contours cluster tightly together indicate the location of the individual fires. The velocities are actually calculated at a height about 0.8 m above the surface. The coordinates and velocities are normalized with respect to the scaling laws introduced in eqs. (20) and (21). The largest individual fire of strength 3.2 MW is used in the non-dimensionalization. The maximum velocity visible at this resolution scale (Figure 19) is approximately 0.8 m/sec. The tick marks on the boundaries are spaced at 1 meter intervals.

Figure 20 shows a local detail magnified ten times in each direction centered near the large fire 3.2 MW (fire #19) about 2/3 of the way to the right and 1/5 up from the bottom of Figure 19. At this resolution, the inflow into the fire plume is clearly visible. Since it is possible to resolve the flow nearer to the plume, the maximum velocity in the fine grid approaches the dimensionless peak inflow velocity for an individual plume U_r in Figure 16. The peak velocity shown in Fig. 20 is about 1.1 m/sec.

Calculations of this type may be extended using idealized wind conditions and measured soot properties to predict convection of the soot produced by the oil spill fires. Basic studies related to the formulation of this more advanced model are presently underway.

TABLE 3. DISTRIBUTION OF FIRE ENERGY RELEASE RATES AND EQUIVALENT PRUDHOE
BAY CRUDE OIL POOL FIRE DIAMETERS USED IN FIGURE 19

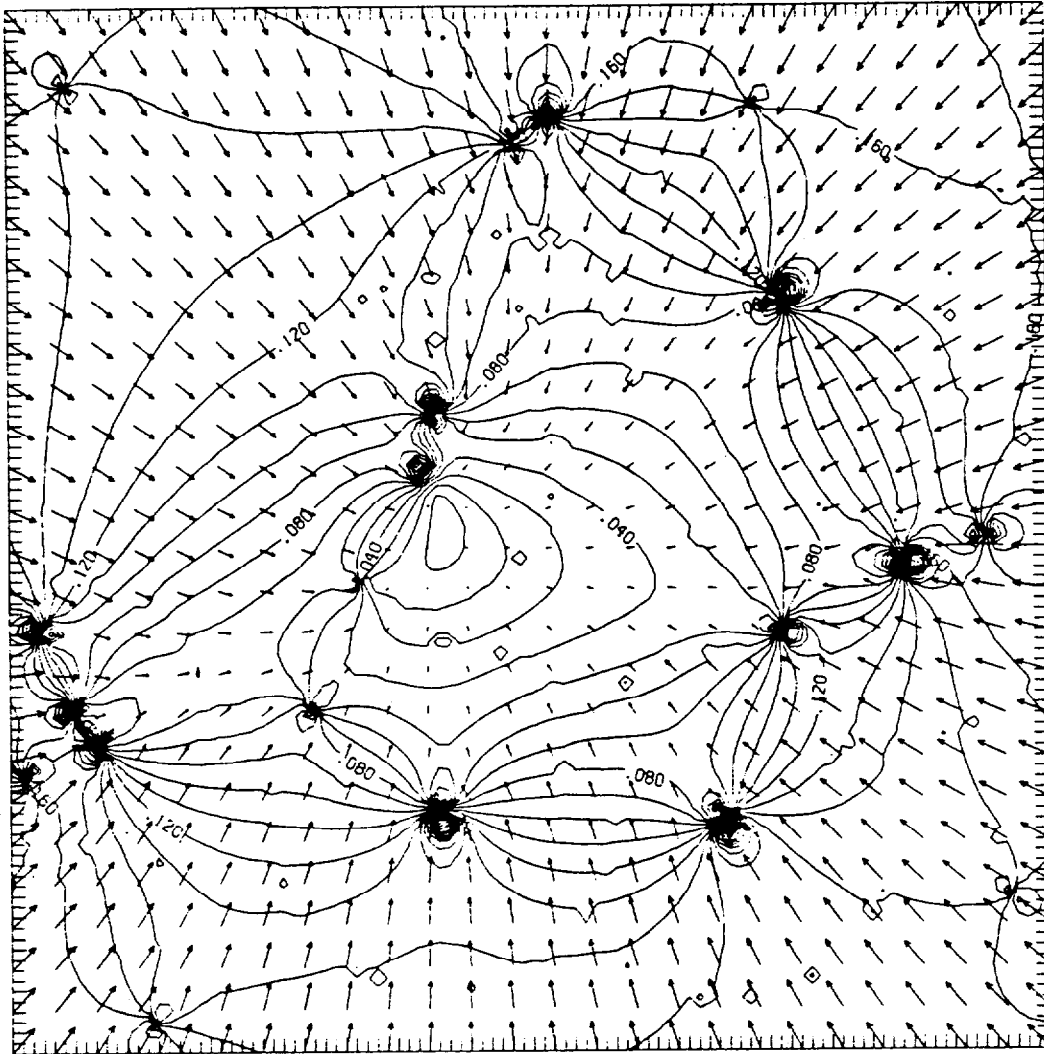| Fire No.	Location X Unit from Left Border (Fig. 19)	Location Y Units from Bottom Border (Fig. 19)	Energy Release Rate kW	Equivalent Pool Diameter m
1	96.613	14.762	200	0.63
2	40.852	61.420	1600	1.78
3	5.483	92.562	200	0.63
4	8.217	29.148	1600	1.78
5	94.120	49.268	800	1.26
6	52.152	89.503	1600	1.78
7	86.683	46.312	3200	2.52
8	39.632	55.463	1600	1.78
9	13.900	2.955	400	0.89
10	33.547	44.622	200	0.63
11	71.857	90.247	200	0.63
12	41.348	22.350	3200	2.52
13	1.095	26.527	800	1.26
14	2.737	40.275	1600	1.78
15	48.530	86.992	800	1.26
16	28.918	32.567	400	0.89
17	74.675	39.835	1600	1.78
18	5.935	32.542	1600	1.78
19	68.680	21.433	3200	2.52
20	74.535	72.075	3200	2.52

FIGURE 19.   COMPOSITE SEA LEVEL INDUCED FLOW GENERATED BY TWENTY RANDOMLY
DISTRIBUTED FIRES RANGING IN STRENGTH FROM 200 KILOWATTS TO
3.2 MEGAWATTS.   THE OVERALL AREA IS 100 METERS ON A SIDE.
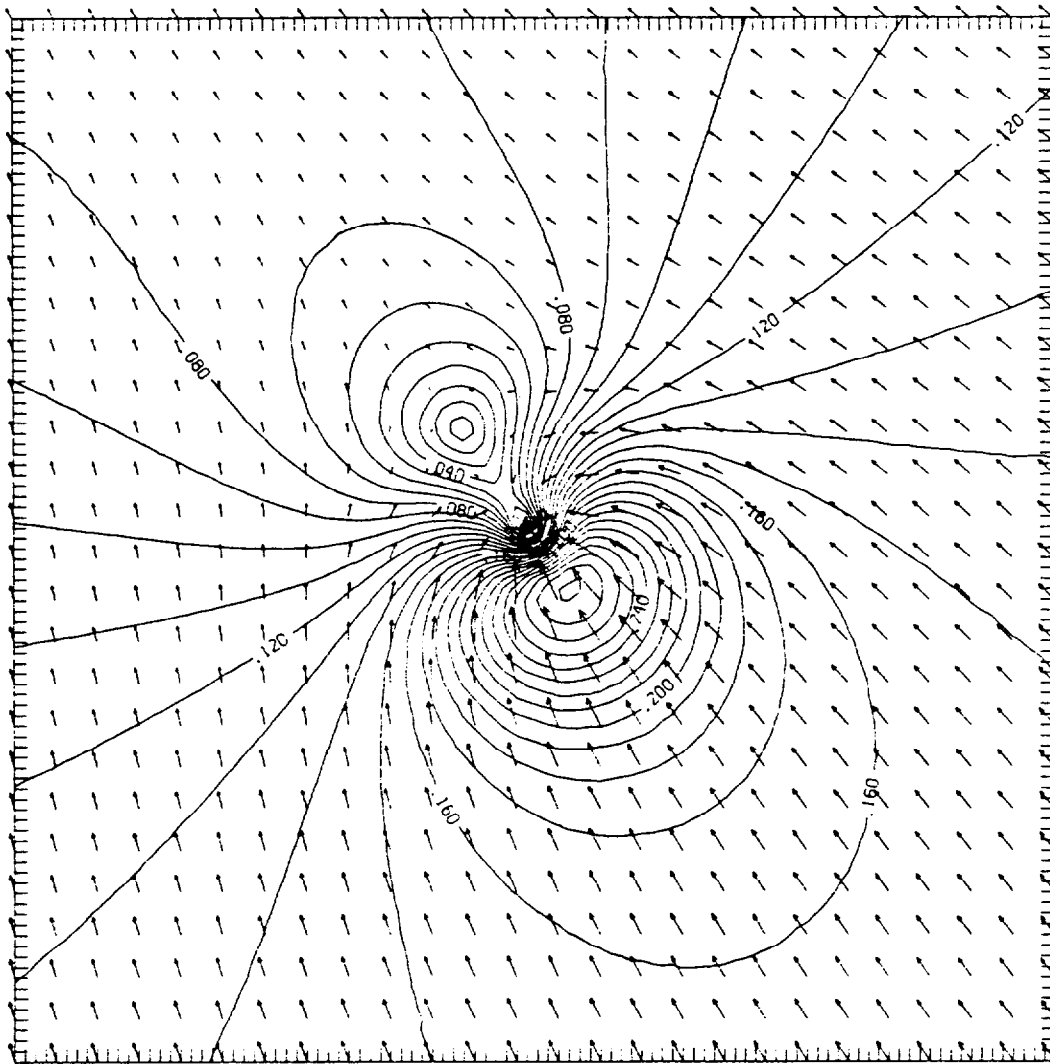VELOCITY RECTORS AND SPEED CONTOURS ARE SHOWN.

FIGURE 20. DETAIL OF VELOCITIES AND SPEED CONTOURS SHOWN IN FIGURE 19
CENTERED NEAR FIRE (FIRE #19, 3.2 MW) 2/3 TO THE RIGHT AND
1/5 UP FROM BOTTOM. SCALE MAGNIFIED 10 TIMES.

REFERENCES

1. Smith, N.K., Diaz, A., "In-Place Burning of Crude Oil in Broken Ice, 1985 Testing at OHMSETT", Proceedings of the Eighth Annual Arctic Marine Oilspill Program Technical Seminar, June 18-20, 1985, Edmonton, Alberta, Technical Services Branch, Environmental Protection Services, Ottawa, Canada K1A 1C8, 176-191 (1985).

2. Wichman, I.S., A Preliminary Analysis of Oil-Slick Combustion, NBSIR 85-3266, U.S. Department of Commerce, National Bureau of Standards, Gaithersburg, MD 20899, November 1985.

3. Huggett, C., Fire and Materials 4, 61 (1980).

4. Thornton, W.M., Philos. Mag. 33, 196 (1917).

5. Babrauskas, V., Smoke Measurement Results from the Cone Calorimeter, Paper presented at United States-Japan Natural Resources (UJNR) meeting, May 1985.

6. Seader, J.D. and Einhorn, I.N., Sixteenth Symp. (International) on Combustion, The Combustion Institute, Pittsburgh, PA, 1423 (1976).

7. Reist, P.C., Introduction to Aerosol Science, New York: Macmillan Publishing Company, Inc., p. 21 (1984).

8. Kualkeim, O.M., Aksnes, D.W., Brekke, T., Eide, M.D., Sletten, E., and Telnaes, N., Anal. Chem. 57, 2858 (1985).

9. Buist, I.A. and Twardus, E.M., "Burning Uncontained Oil Slicks: Large Scale Tests and Modeling", Proceedings of the Eighth Annual Artic Marine Oilspill Program Technical Seminar, June 18-20, 1985, Edmonton, Alberta, Technical Services Branch, Environmental Protection Service, Ottawa, Canada K1A 1C8, 103-130 (1985).

10. Turner, J.S., Buoyancy Effects in Fluids, Cambridge University Press, Cambridge, 8, 1973.

11. McCaffrey, B.J., Momentum Implications for Buoyant Diffusion Flames, Comb. and Flame 52, 149 (1983).